The Cryosphere Discuss., 1, 213–269, 2007
www.the-cryosphere-discuss.net/1/213/2007/

The Cryosphere Discussions

The Cryosphere Discussions is the access reviewed discussion forum of *The Cryosphere*

Estimation of thermal properties of saturated soils using in-situ temperature measurements

D. J. Nicolsky[1], **V. E. Romanovsky**[1], **and G. S. Tipenko**[2]

[1]Geophysical Institute, University of Alaska Fairbanks, PO Box 757320, Fairbanks, AK 99775, USA
[2]Institute of Environmental Geoscience Russian Academy of Sciences, 13-2 Ulansky pereulok, PO Box 145, Moscow, Russia

Received: 1 August 2007 – Accepted: 2 August 2007 – Published: 9 August 2007

Correspondence to: D. J. Nicolsky (ftdjn@uaf.edu)

Abstract

We describe an approach to find an initial approximation to the thermal properties of soil horizons. This technique approximates thermal conductivity, porosity, unfrozen water content curve in horizons where no direct temperature measurements are available. To determine physical properties of ground material, optimization-based inverse modeling techniques fitting the simulated and measured temperatures are commonly employed. Two major ingredients of these techniques is an algorithm to compute the soil temperature dynamics and a procedure to find an initial approximation to the ground properties. In this article we show how to determine the initial approximation to the physical properties and present a new finite element discretization of the heat equation with phase change to calculate the temperature dynamics in soil. We successfully applied the proposed algorithm to recover the soil properties for Happy Valley site in Alaska using one-year temperature dynamics. The determined initial approximation was utilized to simulate the temperature dynamics over several consecutive years; the difference between simulated and measured temperatures lies within uncertainties of measurements.

1 Introduction

Recently, the Arctic Climate Impact Assessment report (ACIA, 2004) concluded that climate change is likely to significantly transform present natural environments, particularly across extensive areas in the Arctic and sub-Arctic. Among the highlighted potential transformations is soil warming which can potentially drive an increase in the active layer thickness and degradation of permafrost as well as have broader impacts on soil hydrology, northern ecosystems and infrastructure. Since permafrost is widely distributed and covers approximately 25% of the land surface in the Northern Hemisphere (Brown et al., 1997), it is very important to understand driving forces affecting soil temperature regime. One of the approaches to study soil temperature

dynamics and its dependence on climate variability is to employ mathematical modeling (Goodrich, 1982; Nelson and Outcalt, 1987; Kane et al., 1991; Zhuang et al., 2001; Ling and Zhang, 2003; Oleson et al., 2004; Sazonova et al., 2004; Molders and Romanovsky, 2006)

A mathematical model of soil freezing/thawing is based on finding a solution of a non-linear heat equation over a certain domain, see (Andersland and Anderson, 1978; Yershov, 1998) and many references therein. The domain represents ground material which has several horizons (e.g. an organic matt, an organically enriched mineral soil layer, and a mineral soil layer) with distinct properties characterized by mineral-chemical composition, texture, porosity, heat capacity and thermal conductivity. By parameterizing coefficients in the heat equation within each horizon using properties of the corresponding layer, it is possible to take into account temperature-dependent latent heat effects occurring when ground freezes and thaws, and hence realistically model temperature dynamics in soils. However, in order to produce quantitatively reasonable results, it is necessary to prescribe physical properties of each horizon accurately. One of the ways to determine these properties is to complete certain laboratory or field experiments (Zhang and Osterkamp, 1995; Yoshikawa et al., 2004). In both cases, it is necessary to solve inverse problems where measured temperature and the model are used to find the parameters within each soil layer.

There is a great number of inverse modeling techniques, but in this article we deal with optimization techniques which fit model output to observations. These techniques find properties $\mathcal{C}$ of all horizons by minimizing the cost function

$$J(\mathcal{C}) \approx \int_{t_s}^{t_e} (T_m(x_i, t) - T_c(x_i, t; \mathcal{C}))^2 dt, \quad (1)$$

which measures a discrepancy between the measured T_m and calculated T_c temperatures (computed by the model with coefficients in the heat equation parameterized using $\mathcal{C}$) at some depths x_i over the time interval $[t_s, t_e]$. Commonly, the cost function J is minimized iteratively starting from an initial approximation to the parameters

$\mathcal{C}$ (Thacker and Long, 1988). Since the heat equation is non-linear, in general there are several local minima. Hence, it is important that the initial approximation lies in the basin of attraction of a proper minimum (Avriel, 2003).

In this article, we present an semi-heuristic algorithm to determine the initial approximation, in order to use it as the starting point in multivariate minimization problems such as (1). We construct the initial approximation by using in-situ measured temperature and by minimizing cost functions on specifically selected time intervals $[t_s, t_e]$ and also in a certain order. For example, first, we propose to find thermal conductivity of the frozen soil using the temperature collected during winter, and then use these values to find properties of the thawed soil. In order to minimize the cost function it is necessary to compute the temperature dynamics multiple times for various $\mathcal{C}$. Since an analytical solution of the non-linear heat equation is not generally available, we use a finite element method to find its solution. To compute latent heat effects, we propose a new fixed grid technique to evaluate the so-called latent heat terms in the so-called mass (compliance) matrix using enthalpy formulation. Our techniques does not rely on temporal or spatial averaging of enthalpy, but rather evaluate integrals directly by employing a certain change of variables. An advantage of this approach is that it allows reductions of the numerical oscillation during evaluation of the temperature dynamics at locations near 0°C isotherm.

The structure of this article is as follows. In Sect. 2, we describe a commonly used mathematical model of temperature changes in the active layer and near surface permafrost. In Section 3, we give a brief review of existing field methods of finding the thermal properties and unfrozen water content. Also, in this section we introduce main definitions and notations. In Sect. 4, we outline a finite element discretization of the heat equation with phase change. In Sect. 5, we provide an algorithm to construct an initial approximation to thermal properties. In Section 6, we outline global minimization of the cost function. In Sect. 7, we apply our method to estimate the thermal properties and the coefficients determining the unfrozen water content at a site located in Alaska. Finally, in Sect. 8 we present limitations and shortcomings of the proposed algorithm.

2 Modeling of soil freezing and thawing

For many practical applications, heat conduction is a dominant process, and hence the soil temperature T, [°C] can be simulated by a 1-D heat equation with phase change (Carslaw and Jaeger, 1959):

$$C\frac{\partial}{\partial t}T(x,t) + L\frac{\partial}{\partial t}\theta_l(T,x) = \frac{\partial}{\partial x}\lambda\frac{\partial}{\partial x}T(x,t), \quad (2)$$

where $x \in [0, l]$, $t \in [0, \tau]$; the quantities $C=C(T,x)$ $[Jm^{-3}K^{-1}]$ and $\lambda=\lambda(T,x)$ $[Wm^{-1}K^{-1}]$ stand for the volumetric heat capacity and thermal conductivity of soil, respectively; L $[Jm^{-3}]$ is the volumetric latent heat of fusion of water, and θ_l is the volumetric water content. We note that this equation is applicable when migration of water is negligible, there are no internal sources or sinks of heat, frost heave is insignificant, and there are no changes in topography and soil properties in lateral directions. Typically, the heat Eq. (2) is supplemented by boundary conditions specified at the ground surface, $x=0$, and at the depth l (Carslaw and Jaeger, 1959). For example, the boundary conditions can be given by $T(0,t)=T_u(t)$, $T(l,t)=T_l(t)$, where T_u and T_l are some functions of time and represents temperature at the ground surface and at the depth l, respectively. In order to calculate the temperature dynamics $T(x,t)$ at any time $t \in [0,\tau]$, Eq. (2) is supplemented by an initial condition, i.e. $T(x,0)=T_0(x)$, where $T_0(x)$ is the temperature at $x \in [0,l]$ at time $t=0$.

In certain conditions such as waterlogged Arctic lowlands, soil can be considered a porous media fully saturated with water. The fully saturated soil is a multi-component system consisting of soil particles, liquid water, and ice. It is known that the energy of the multi-component system is minimized when a thin film of liquid water (at temperature below 0°C) separates ice from the soil particles (Hobbs, 1974). A film thickness depends on soil temperature, pressure, mineralogy, solute concentration and other factors (Hobbs, 1974). One of the commonly used measures of liquid water below freezing temperature is *the volumetric unfrozen water content* (Williams, 1967; Anderson and Morgenstern, 1973; Osterkamp and Romanovsky, 1997; Watanabe and

Mizoguchi, 2002). It is defined as the ratio of liquid water volume in a representative soil domain at temperature T to the volume of this representative domain and is denoted by $\theta_l(T)$. In the fully saturated soil $\theta_l(T)$ can be parameterized by a power function $\theta_l(T)=a|T|^{-b}$; $a, b>0$ for $T<T_*<0^\circ$C (Lovell, 1957). The constant T_* is called the freezing point depression (Hobbs, 1974), and from the physical point of view it means that ice does not exist in the soil if $T>T_*$. In thawed soils ($T>T_*$), the amount of water in the saturated soil is equal to the soil porosity η, and hence the function $\theta_l(T)$ can be extended to $T>T_*$ as $\theta_l(T)=\eta$. Therefore, we assume that

$$\theta_l(T,x)=\eta(x)\phi(T,x), \quad \phi=\begin{cases}1, & T\geq T_*\\ |T_*|^b|T|^{-b}, & T<T_*\end{cases}, \tag{3}$$

where $\phi=\phi(T,x)$ represents the soil saturation. Note that the constants T_* and b are the only parameters that specify dependence of the unfrozen liquid water on temperature. For example, small values of b describe the liquid water content in some fine-grained soils, whereas large values of b are related to coarse-grained materials in which almost all water freezes at the temperature T_*. The limiting case in which all water freezes at the temperature T_* is associated with phase change between water and ice (no soil particles). This limiting case is commonly called the classical Stefan problem and is represented by extremely large values of b in (3).

In this article, we use the following notation and definitions. We abbreviate by letters i, l and s, ice, liquid water, and the soil particles, respectively. We express thermal conductivity λ of the soil and its apparent volumetric heat capacity C_{app} according to (de Vries, 1963; Sass et al., 1971) as

$$\lambda(T)=\lambda_s^{\theta_s}\lambda_i^{\theta_i(T)}\lambda_l^{\theta_l(T)}, \quad C_{\text{app}}(T)=C(T)+L\frac{d\theta_l(T)}{dT} \tag{4}$$

$$C(T)=\theta_i(T)C_i+\theta_l(T)C_l+\theta_sC_s \tag{5}$$

where C is called the volumetric heat capacity of the soil. Here, the constants C_k, λ_k, $k \in \{i, l, s\}$ are the volumetric heat capacity and thermal conductivity of the k-th constituent, respectively. The quantity θ_k, $k \in \{i, l, s\}$ is the volume fraction of each constituent. Exploiting the relations $\theta_s = 1-\eta$ and $\theta_i = \eta - \theta_l$, we introduce notation for the effective volumetric heat capacities C_f and C_t, and the effective thermal conductivities λ_f and λ_t of soil for frozen and thawed states, respectively. Therefore formulae (4) and (5) yield

$$C_{\text{app}} = C + L\frac{d\theta_l}{dT}, \quad C = C_f(1-\phi) + C_t\phi, \quad \lambda = \lambda_f^{1-\phi}\lambda_t^{\phi}, \tag{6}$$

where

$$\lambda_f = \lambda_s^{1-\eta}\lambda_i^{\eta}, \quad \lambda_t = \lambda_s^{1-\eta}\lambda_l^{\eta}$$

$$C_f = C_s(1-\eta) + C_i\eta, \quad C_t = C_s(1-\eta) + C_l\eta.$$

For most soils, seasonal deformation of the soil skeleton is negligible, and hence temporal variations in the total soil porosity η for each layer are insignificant. Therefore, the thawed and frozen thermal conductivities for the *fully saturated soil* satisfy

$$\frac{\lambda_t}{\lambda_f} = \left[\frac{\lambda_l}{\lambda_i}\right]^{\eta}. \tag{7}$$

It is important to emphasize that evaporation from the ground surface and from within the upper organic layer can cause partial saturation of upper soil horizons (Hinzman et al., 1991; Kane et al., 2001). Therefore, formula (7) need not hold within live vegetation and organic soil layers, and possibly within organically enriched mineral soil (Romanovsky and Osterkamp, 1997).

In this article, we approximate the coefficients C_{app}, λ according to (6), where the thermal properties $\lambda_f, \lambda_t, C_f, C_t$ and parameters η, T_*, b are constants within each soil horizon. Table 1 lists typical soil horizon geometry, commonly occurring ranges for the porosity η, thermal conductivity λ_f and the values of b parameterizing the unfrozen water content.

3 Review of existing methods utilized to estimate soil physical properties and a short description of our approach

Conventional Time Domain Reflectometry (Topp et al., 1980) and drying methods are commonly used to estimate soil water content at shallow depths. The Time Domain Reflectometry method is based on measurements of the apparent dielectric constant around a wave guide inserted into the soil. It has been demonstrated that there is a relationship between the apparent dielectric constant and liquid water content (Topp et al., 1980) enabling robust estimations of water content in shallow soils with homogeneous composition. There are some difficulties however in measuring θ_l of coarsely textured, heterogeneous or organically enriched soils in Arctic tundra (Boike and Roth, 1997; Yoshikawa et al., 2004). More accurate measurements of the total water content (ice and water together) can be accomplished by thermalization of neutrons and gamma ray attenuation. This is not always suitable for Arctic regions as it requires transportation of radioactive equipment (Boike and Roth, 1997). An alternative to the above-mentioned methods and also to a number of others (Schmugge et al., 1980; Tice et al., 1982; Ulaby et al., 1982; Stafford, 1988; Smith and Tice, 1988) is inverse modeling techniques. These techniques estimate the water content and other thermal properties of soil using *in-situ temperature measurements* and by exploiting *the mathematical model* (2).

A variety of inverse modeling techniques that recover the thermal properties of soil are known. Many of them rely on the commonly called source methods (Jaeger and Sass, 1964), where a temperature response due to heating by a probe is measured at a certain distance away from the probe. The temperature response and geometry of the probe are used to compute the thermal properties by either direct or indirect methods. In the direct methods, the temperature measurements are explicitly used to evaluate the thermal properties. In the indirect methods, one minimizes a discrepancy between the measured and *the synthetic temperatures*, the latter computed via a mathematical model for certain values of the thermal properties.

Application of direct methods such as the Simple Fourier Methods (Carson, 1963), Perturbed Fourier Method (Hurley and Wiltshire, 1993), and the Graphical Finite Difference Method (McGaw et al., 1978; Zhang and Osterkamp, 1995; Hinkel, 1997) to estimate coefficients in (2) yield accurate results for the thermal diffusivity λ/C, only when the phase change of water does not occur. Despite the fact that the direct methods are well established for the heat equation without the phase change, no universal framework exists in the case of the soil freezing/thawing because the heat capacity $C_{\text{app}}(T)$ and thermal conductivity $\lambda(T)$ in this case depend strongly on the temperature T in the heat Eq. (2).

A common implementation of the indirect methods uses an analytical or numerical solution of the heat Eq. (2) to evaluate the synthetic temperature. Due to strong nonlinearities, the analytical solution of (2) is known only for a limited number of cases (Gupta, 2003), while the numerical solution is typically always computable. Given a numerical solution computed by finite difference (Samarskii and Vabishchevich, 1996) or finite element (Zienkiewicz and Taylor, 1991) methods, one can minimize a cost function describing the discrepancy between the measured and synthetic temperatures. The cost function is commonly defined as a sum of squared differences between the calculated and measured temperatures at the several depths and is used to implicitly evaluate the thermal properties (Alifanov et al., 1996). Mathematically, this method can be stated as follows.

We define the *control* $\mathcal{C}$ as a set consisting of thermal conductivities $\lambda_t^{(i)}, \lambda_f^{(i)}$, heat capacities $C_t^{(i)}, C_f^{(i)}$ and parameters $\eta^{(i)}, T_*^{(i)}, b^{(i)}$ describing the unfrozen water content for each soil horizon $i=1,\ldots,n$, or

$$\mathcal{C} = \{C_f^{(i)}, C_t^{(i)}, \lambda_t^{(i)}, \lambda_f^{(i)}, \eta^{(i)}, T_*^{(i)}, b^{(i)}\}_{i=1}^{n}, \tag{8}$$

where n is the total number of horizons. We say that a solution of *the direct problem* for the control $\mathcal{C}$ is $T(x,t;\mathcal{C})$ and is defined by the set

$$T(x,t;\mathcal{C}) = \{T(x_i,t) : i = 1,\ldots,m; t \in [0,\tau]\}, \tag{9}$$

where x_i are some fixed distinct points on $[0, l]$. In (9), the $T(x_i, t)$ are point-wise values of temperature distributions satisfying (2) in which thermal properties of each horizon are given according to $\mathcal{C}$.

The so-called counterpart of $T(x, t; \mathcal{C})$ is the *data* $T_{\mathcal{D}}(x, t)$ defined by a set of measured temperature at the same depths $\{x_i\}_{i=1}^{m}$ and the same time interval $[0, \tau]$. Since the data $T_{\mathcal{D}}(x, t)$ and its model counterpart $T(x, t; \mathcal{C})$ are given on the same set of depths and time interval, we can easily compute a discrepancy between them, usually measured by the cost function

$$J(\mathcal{C}) = \frac{1}{m(t_s - t_e)} \sum_{i=1}^{m} \frac{1}{\sigma_i^2} \int_{t_s}^{t_e} (T_{\mathcal{D}}(x_i, t) - T(x_i, t; \mathcal{C}))^2 dt. \tag{10}$$

Here, $t_s, t_e \in [0, \tau]$ and σ_i stands for an uncertainty in measurements by the i-th sensor. In our measurements all temperature sensors assume the same precision, so all of $\{\sigma_i\}$ are equal. Given a way to measure this discrepancy as in (10) we can finally formulate an inverse problem.

For the given data $T_{\mathcal{D}}(x, t)$, we say that the control $\mathcal{C}_*$ is a solution to *an inverse problem* if discrepancy between the data and its model counterpart evaluated at $\mathcal{C}_*$ is minimal (Alifanov, 1994; Alifanov et al., 1996; Tikhonov and Leonov, 1996). That is,

$$\mathcal{C}_* = arg \min_{\mathcal{C}} J(\mathcal{C}).$$

To illustrate steps which are necessary to solve this inverse problem and find an optimal $\mathcal{C}_*$ we provide the following example. To formulate the inverse problem one has to have the measured temperatures $T_{\mathcal{D}}(x, t)$. For the sake of this example, we replace the data $T_{\mathcal{D}}(x, t)$ by a synthetic temperature $T_{\mathcal{S}}(x, t) = T(x, t; \mathcal{C}')$ (a numerical solution of the heat Eq. (2) for the known combination $\mathcal{C}'$ of the thermal properties):

$$\mathcal{C}' = \left\{ \begin{array}{l} c_f^{(1)}=1.6\cdot10^6,\ c_t^{(1)}=2.1\cdot10^6,\ \lambda_f^{(1)}=0.55,\ \lambda_t^{(1)}=0.14,\ \eta^{(1)}=0.30,\ b^{(1)}=-0.9,\ T_*^{(1)}=-0.03 \\ c_f^{(2)}=1.7\cdot10^6,\ c_t^{(2)}=2.3\cdot10^6,\ \lambda_f^{(2)}=\mathbf{0.90},\ \lambda_t^{(2)}=0.66,\ \eta^{(2)}=0.30,\ b^{(2)}=-0.6,\ T_*^{(2)}=-0.03 \\ c_f^{(3)}=1.8\cdot10^6,\ c_t^{(3)}=2.6\cdot10^6,\ \lambda_f^{(3)}=1.90,\ \lambda_t^{(3)}=1.25,\ \eta^{(3)}=\mathbf{0.25},\ b^{(3)}=-0.8,\ T_*^{(3)}=-0.03 \end{array} \right\}.$$

The initial and boundary conditions in all calculations are fixed and given by in-situ temperature measurements in 2001 and 2002 at the Happy Valley site located in the Alaskan Arctic. We compute the temperature dynamics for a soil slab with dimensions $[0.02, 1.06]$ between 21 July 2001 and 6 May 2002, and evaluate the cost function at $\{x_i\}_i$=$\{0.10, 0.17, 0.25, 0.32, 0.40, 0.48, 0.55, 0.70, 0.86\}$ meters. Uniformly distributed noise on $[-0.04, 0.04]$ was added to $T_{\mathcal{S}}(x,t)$, to simulate noisy temperature data recorded by sensors (precision of the sensor is 0.04°C).

Given the synthetic data $T_{\mathcal{S}}(x,t)$, we can find a best choice of parameters to minimize the cost function J defined by (10), where $T_{\mathcal{D}}(x,t)$=$T_{\mathcal{S}}(x,t)$. For the sake of simplicity, we assume that all parameters in the controls $\mathcal{C}'$ are known except for the pair $\lambda_f^{(2)}, \eta^{(3)}$. Therefore, the problem of finding this pair can be solved by minimizing the two-parameter-dependent cost function as follows. First, we compute temperature dynamics for all possible combinations of $\lambda_f^{(2)}, \eta^{(3)}$ on a discrete grid of values of these parameters. Second, for each combination of the pair, we evaluate the cost function $J(\mathcal{C})$ and plot its isolines on $(\lambda_f^{(2)}, \eta^{(3)})$ plane. Finally, at the third step, we look for a minimum of the cost function and determine a location of its minimum. The point on $(\lambda_f^{(2)}, \eta^{(3)})$ plane where the cost function is minimal gives the sought values of $\lambda_f^{(2)}$ and $\eta^{(3)}$. Figure 1 shows typical contours of the isolines in the vicinity of the unique minimum. We see that the location of the minimum coincides with values $\lambda_f^{(2)}$=0.9, $\eta^{(3)}$=0.25, which were used to generate the synthetic data.

In the above example, the control had only two unknown variables $\lambda_f^{(2)}, \eta^{(3)}$ and we minimized the corresponding cost function. Usually, a majority of variables in the control $\mathcal{C}$ is unknown, and hence multivariate minimization is required. Since computation of the cost function for all possible realizations of the control on the discrete grid is extremely time-consuming, various iterative techniques are used (Fletcher, 2000). In any iterative technique, an initial approximation to the variables is needed, and the choice of the initial approximation is extremely important to save computational time and increase accuracy. For instance, if the cost function has several minima due to

non-linearities of the heat Eq. (2) and if the initial approximation is arbitrary then the iterative algorithm can converge to an improper minimum. Nevertheless, with the initial approximation/guess within the basin of attraction of the global minimum, the iterative optimization method should converge to the proper minimum even if the model is nonlinear (Thacker, 1989). To estimate the thermal properties uniquely (a unique minimum), the boundary conditions must satisfy some requirements, e.g.be monotonous functions of time (Muzylev, 1985). In nature, rapidly changing weather conditions drive the surface temperature which does not fulfil the necessary requirements for existence of the unique minimum. Consequently, proper determination of an initial approximation is extremely important. In addition to the proper determination of the initial approximation, it is also important to compute the temperature dynamics for various combinations of thermal properties with high efficiency. In the next two following sections, we propose a new highly efficient numerical method for solving the heat equation and provide a recipe for the selection of an initial approximation.

4 Solution of the heat equation with phase change

4.1 A review of numerical methods

In order to solve the inverse problem one needs to compute a series of direct problems, i.e. to obtain the temperature fields for various combinations of thermal properties. A number of numerical methods (Javierre et al., 2006) exist to compute temperature that satisfies the heat equation with phase change (2). These methods vary from the simplest ones which yield inaccurate results to sophisticated ones which produce accurate temperature distributions. The highly sophisticated methods explicitly track a region where the phase change occurs and produce a grid refinement in its vicinity, and therefore take significantly more computational time to obtain temperature dynamics. Implementing such complicated methods is not always necessary, since an extremely accurate solution is not particularly important when the mathematical model describing

nature is significantly simplified.

In this subsection, we briefly review several fixed grid techniques (Voller and Swaminathan, 1990) that accurately estimate soil temperature dynamics and easily extend to multi-dimensional versions of the heat Eq. (2). These methods provide the solution for arbitrary temperature-dependent thermal properties of the soil and do not explicitly track the area where the phase change occurs. Recall that in soils the phase change occurs at almost all sub-zero temperatures. A cornerstone of the fixed grid techniques is a numerical approximation of the apparent heat capacity C_{app}. A variety of the approximation techniques can be found in (Voller and Swaminathan, 1990; Pham, 1995) and references therein. In general, two classes of them can be identified. The first class is based on temperature/coordinate averaging (Comini et al., 1974; Lemmon, 1979) of the phase change. Here, the apparent heat capacity is approximated by

$$C_{app} = \frac{\partial H}{\partial x}\left(\frac{\partial T}{\partial x}\right)^{-1}, \tag{11}$$

where

$$H = \int_0^T C_{app} dT,$$

is the enthalpy. The second class of methods is based on temperature/time averaging (Morgan et al., 1978). In this approach,

$$C_{app} = \frac{H_{current} - H_{previous}}{T_{current} - T_{previous}}, \tag{12}$$

where subscripts mark time steps at which the values of H and T are calculated. Although these methods have been presented in the context of large values of b in (3), it is noted that they work best in the case of a naturally occurring wide phase change interval. Also, it is important to note that the approximation (11) is not accurate for

near zero temperature gradients. In the case when the boundary conditions are given by natural climate variability (several seasonal freezing/thawing cycles), near zero gradients at some depths may occur for some time intervals. Hence, the temperature dynamics calculated by using (11) can have large computational errors.

An alternative fixed grid technique can be developed by rewriting the heat equation (2) in a new form:

$$\frac{\partial H}{\partial t} = \frac{\partial}{\partial x}\lambda\frac{\partial}{\partial x}T, \quad T = T(H), \tag{13}$$

resulting in the enthalpy diffusion method (Mundim and Fortes, 1979). Advantages of discretizing (13) is that the temperature $T=T(H)$ is a smooth function of enthalpy H and hence one can compute all partial derivatives. However, for soils with a sharp boundary between thawed and completely frozen states, the enthalpy H becomes a multivariate function when temperature T nears T_*. Therefore, solution of (13) results in that the front becomes artificially stretched over at least one or even several finite elements.

In this article, we propose a fixed grid method that uses the standard finite element method. Application of the standard finite element method to the left hand side of (2) results in

$$\int_{x_0}^{x_1} \psi(x)\frac{d\theta_l}{dT}(T(x,t))dx,$$

where $\psi(x)$ is a product of two finite element basis functions, and $T(x,t)$ is the temperature at the point x and time t. We propose to evaluate this type of integrals using the unfrozen liquid water content θ_l as the integration variable, i.e.

$$\int_{x_0}^{x_1} \psi(x)\frac{d\theta_l}{dT}(T(x,t))dx = \int_{\theta_0}^{\theta_1} \psi(T(\theta_l,t))d\theta_l, \tag{14}$$

where $\theta_0 = \theta_l(T(x_0,t))$ and $\theta_1 = \theta_l(T(x_1,t))$. This substitution allows precise computation of the latent heat effect for arbitrary grid cells, since it is parameterized by the

limits of integration θ_0, θ_1, instead of being calculated using the rapidly varying function $\frac{d\theta_l}{dT}(T)$ on the element $[x_0, x_1]$ by a quadrature rule. To apply the proposed substitution, the function $T(\theta_l)$ must be monotonically increasing for all $\theta_l < \eta$. Figure 2 shows two instances of the unfrozen water content curves frequently occurring in nature. The curve marked by circles is associated with soils in which free water freezes prior to freezing of the bound liquid water in soil pores. The free water is associated with a vertical line at $T = T_*$ whereas the bound water is represented by a smooth curve at $T < T_*$. The curve marked by triangles reflects soil in which all water is bounded in soil pores and can be parameterized by (3) used in our modeling.

4.2 Finite element formulation

Let us consider a triangulation of the interval $[0, l]$ by a set of nodes $\{x_i\}_{i=1}^n$. With each node x_i, we associate a continuous function $\psi_i(x)$ such that $\psi_i(x_j) = \delta_{ij}$. We will refer to $\{\psi_i\}_{i=1}^n$ as the basis functions on the interval $[0, l]$. Hence, the temperature $T(x, t)$ on $[0, l]$ is approximated by a linear combination: $T(x, t) = \sum_{i=1}^n T_i(t)\psi_i(x)$, where $T_i = T_i(t)$ is the temperature at the node x_i at the time t. Substituting this linear combination into (2), multiplying it by ψ_j and then integrating over the interval $[0, l]$, we obtain a system of differential equations (Zienkiewicz and Taylor, 1991):

$$\mathbf{M}(\mathbf{T})\frac{d}{dt}\mathbf{T}(t) = -\mathbf{K}(\mathbf{T})\mathbf{T}(t), \tag{15}$$

where $\mathbf{T} \equiv \mathbf{T}(t) = [T_1(t)\ T_2(t)\ \ldots T_n(t)]^t$ is the vector of temperatures at nodes $\{x_i\}_{i=1}^n$ at time t. Here, the $n \times n$ matrices $\mathbf{M}(\mathbf{T}) = \{m_{ij}\}_{ij=1}^n$ and $\mathbf{K}(\mathbf{T}) = \{k_{ij}\}_{ij=1}^n$ are mass and stiffness matrices, respectively. Entry-wise they are defined as

$$m_{ij} = \int_0^l C(T, x)\psi_i\psi_j dx + L\int_0^l \frac{d\theta_l}{dT}\psi_i\psi_j dx \tag{16}$$

$$k_{ij} = \int_0^l \lambda(T, x)\frac{d\psi_i}{dx}\frac{d\psi_j}{dx}dx. \tag{17}$$

The fully implicit scheme is utilized to discretize (15) with respect to time. Denoting by dt_k the time increment at the k-th moment of time t_k, one has

$$\left[\mathbf{M}^k + dt_k \mathbf{K}^k\right]\mathbf{T}^k = \mathbf{M}^k \mathbf{T}^{k-1}, \quad k > 1 \tag{18}$$

where $\mathbf{T}^k$=$\mathbf{T}(t_k)$, $\mathbf{K}^k$=$\mathbf{K}(\mathbf{T}^k)$, $\mathbf{M}^k$=$\mathbf{M}(\mathbf{T}^k)$. We impose boundary conditions at x=0 and some depth x=l by specifying $T_1(t_k)$=$T_u(t_k)$ and $T_n(t_k)$=$T_l(t_k)$.

Given $\mathbf{T}^{k-1}$, we find the solution $\mathbf{T}^k$ of (18) by Picard iteration. The iteration process starts from the initial guess $\mathbf{T}^k_0$=$\mathbf{T}^{k-1}$ that is used to compute temperature $\mathbf{T}^k_1$ at the first iteration. At iteration s, we compute $\mathbf{T}^k_s$ and terminate iterations at s_e when a certain convergence condition is met. The value of $\mathbf{T}^k_s$ is used to evaluate the matrices $\mathbf{M}^k{}_s$=$\mathbf{M}(\mathbf{T}^k_s)$, and $\mathbf{K}^k{}_s$=$\mathbf{K}(\mathbf{T}^k_s)$. In turn, these are utilized to compute the $s+1$ iteration $\mathbf{T}^k_{s+1}$ by equating

$$[\mathbf{M}^k{}_s + dt_k \mathbf{K}^k{}_s]\mathbf{T}^k{}_{s+1} - \mathbf{M}^k{}_s \mathbf{T}^{k-1} = 0. \tag{19}$$

At each iteration the convergence condition $\max_k |T^{s+1}_k(t_k) - T^s_k(t_k)| \le \epsilon$ is checked. If it hold, the iterations are terminated at s_e=s+1. If the number of iterations exceeds a certain predefined number, the time increment dt_k is halved and the iterations start again. Please, note that the convergence is guaranteed if the time increment dt_k is small enough.

4.3 Computation of the mass matrix

One of the obstacles to obtain a finite dimensional approximation that accurately captures the temperature dynamics is related to evaluation of the mass matrix $\mathbf{M}$. Since the basis function ψ_i does not vanish only on the interval $[x_{i-1}, x_{i+1}]$, the matrix $\mathbf{M}$ is tri-diagonal. Therefore, to compute its i-th row we evaluate

$$\int_0^l \frac{d\theta_l}{dT}\psi_j(x)\psi_i(x)dx \quad j = i-1, i, i+1, \tag{20}$$

where j stands for the column index. For the sake of brevity, we consider the first integral ($j=i-1$) in (20). This restricts us only to the grid element $[x_{i-1}, x_i]$, yielding

$$\int_0^l \frac{d\theta_l}{dT}\psi_{i-1}(x)\psi_i(x)dx = \int_{x-1}^{x_i} \frac{d\theta_l}{dT}\psi_{i-1}(x)\psi_i(x)dx. \quad (21)$$

We recall that in the standard finite element method, the temperature on the interval $[x_{i-1}x_i]$ is approximated by

$$T(x,t)=\psi_{i-1}(x)T_{i-1}(t)+\psi_i(x)T_i(t), \quad (22)$$

for any $x \in [x_{i-1}, x_i]$ and fixed moment time t. Here, ψ_i and ψ_{i-1} are piece-wise linear functions satisfying $\psi_{i-1}=1-\psi_i$ on $[x_{i-1}, x_i]$. For all $x \in [x_{i-1}, x_i]$, we can compute the temperature T from (22) and values of T_i, T_{i-1}. Note that in the case of $\Delta T_i=0$, we can compute (21) directly since $d\theta_l/dT$ is constant over $[x_{i-1}x_i]$. However, if $\Delta T_i=T_i-T_{i-1} \neq 0$, then we can consider an inverse function, that is, x is taken as a function of T to obtain

$$\int_{x_{i-1}}^{x_i} \frac{d\theta_l}{dT}\psi_{i-1}\psi_i dx = \frac{x_i - x_{i-1}}{(\Delta T_i)^3}\int_{x_{i-1}}^{x_i} \frac{d\theta_l}{dT}(T_i - T)(T - T_{i-1})dT$$

Therefore

$$\int_0^l \frac{d\theta_l}{dT}\psi_{i-1}\psi_i\, dx = \frac{x_i - x_{i-1}}{(\Delta T_i)^3}\int_{\theta_{i-1}}^{\theta_i} (T - T_i)(T_{i-1} - T)d\theta, \quad (23)$$

where $\theta_{i-1}=\theta_l(T(x_{i-1},t))$ and $\theta_i=\theta_l(T(x_i,t))$. Note that in (23) the temperature T is a function of the liquid water content θ_l, i.e. $T=\theta_l^{-1}(\theta_l)$. Therefore, returning back to (20), we have that each of the integrals in (20) is a linear combination of the type $\beta_2 A_2 + \beta_1 A_1 + \beta_0 A_0$, where

$$A_k = \int_{\theta_{i-1}}^{\theta_i} [\theta_l^{-1}(z)]^k dz, \quad k = 0, 1, 2.$$

The constants $\{\beta_k\}$ are easily computable if $\theta_l(T)$ is given by (3).

4.4 Evaluation of the proposed method

To test the proposed method, we compare temperature dynamics computed by the proposed method with an analytical solution of the heat Eq. (2) in which $b \rightarrow \infty$. This analytical solution is called Neumann solution (Gupta, 2003) and is typically used to verify numerical schemes. In the proposed numerical scheme the mass matrix **M** is tri-diagonal, and hence this scheme is called consistent. Other commonly utilized numerical schemes are called mass lumped (Zienkiewicz and Taylor, 1991) since they employ the diagonal mass matrix:

$$\mathbf{M} = \mathrm{diag}(C_{\mathrm{app},1} \int_0^1 \psi_1 dx, \ldots, C_{\mathrm{app},n} \int_0^1 \psi_n dx). \quad (24)$$

Here, $C_{\mathrm{app},i}$ is the value of the apparent heat capacity C_{app} at the $i-$th node computed either by spatial (11) or temporal (12) averaging of latent heat effects.

In Fig. 3, we compare temperature dynamics computed by the proposed consistent and a typical mass lumped scheme. We plot a location of the 0°C isotherm for several spatial discretizations, i.e. the distance Δx_i between two neighboring nodes x_i and x_{i-1} is 0.1 or 0.01 meter. In this figure we see that the location of the 0°C isotherm calculated by numerical schemes lies within Δx_i bound near the analytical solution. However, temporal dynamics of the location of the 0°C isotherm differ among methods. In the solution (squares) computed by the mass lumped approach with temporal enthalpy averaging (TA), dynamics of the 0°C isotherm has some irregularities, i.e. the freezing front either advancing too fast or too slow. In average, however this algorithm produces good results. Our proposed consistent method (circles) gives a better solution and smoother rate of advancing of the 0°C isotherm, see Fig. 3, left.

In Fig. 4, we compare temperature dynamics computed by two mass lumped approaches exploiting spatial (11) and temporal (12) enthalpy averaging. A warm bias in the temperature computed by the spatial averaging of the enthalpy is due to computational errors occurring when the temperature gradient is approximately zero at some

depth. Our experience shows that this difference appears regardless of decreasing the tolerance ϵ between iterations in (19). We note that in all above numerical experiments a finite element computer code is the same except for a part associated with computation of mass matrix, i.e. consistent (20) or mass lumped (24). These numerical experiments show that the straight-forward mass lumped schemes are typically inferior to consistent ones.

Since our method (16) is based on the consistent approach (the mass matrix $\mathbf{M}$ is the tri-diagonal one), the numerical solution oscillates if the time steps dt_k are too small (Pinder and Gray, 1977). For a fixed time step dt_k, the oscillations disappear if the spatial discretization becomes fine. It is shown that these oscillations occur due to violation of the so-called discrete maximum principle (Rank et al., 1983). Therefore, to avoid the oscillations in the numerical solution (Dalhuijsen and Segal, 1986), we propose either to use sufficiently large time steps (for which the formula can be found in the above cited references) or to exploit the following regularization. We construct a lumped version $\tilde{\mathbf{M}}=\{\tilde{m}_{ij}\}$ of the mass matrix $\mathbf{M}$ given by

$$\tilde{m}_{ij} = \sum_j m_{ij} \tag{25}$$

and substitute $\tilde{\mathbf{M}}$ for $\mathbf{M}$ in (18). Comparison of temperature dynamics computed employing the proposed consistent $\mathbf{M}$ defined by (18) and its mass lumped modification $\tilde{\mathbf{M}}$ defined by (25) is shown in Fig. 5. The numerical oscillations near 0°C disappear in the temperature dynamics computed by the proposed mass lumped approach (see Fig. 5). In Fig. 6, we compare the proposed mass lumped approach (stars), and the one based on temporal enthalpy averaging (squares) by (11). This figure shows that the numerical scheme using temporal averaging of the enthalpy produces larger oscillation than our solution. This comparison reveals that the proposed mass lumped approach (25) reduces some numerical oscillations and follows the "exact" solution (computed by the consistent approach with a very fine spatial discretization) more closely than the solution computed by the lumped approach exploiting (11).

In conclusion, we state that if a spatial discretization is fine and time steps are sufficiently large (Pinder and Gray, 1977) then the consistent schemes do not show numerical oscillations, and hence they should be utilized. In the case of a coarse spatial discretization, consistent schemes can violate the discrete maximum principle, and hence the mass lumped schemes are more attractive. In this article, we construct a fine spatial discretization and use the proposed consistent approach, while restricting the time step t_k from below.

5 Selection of an initial approximation

As it was mentioned previously, selection of a proper initial approximation is crucial to reduce the number of iterations and more importantly to ensure that the minimization procedure converges to a global minimum. In this section we describe how to select a proper initial approximation. Note that in the natural environment, the thermal properties and the water content are confined within a certain range varying from soil texture and mineralogy. Therefore, the coefficients in (2) and hence their initial approximations lie within certain limits. To ensure better determination of *the initial approximation*, we employ an algorithm utilizing coordinate-wise searching (Bazaraa et al., 1993). This algorithm looks for a minimum along one coordinate, keeping all other parameters fixed, and then looks for the minimum along another coordinate keeping all others fixed and so on. We propose a similar algorithm to establish the initial approximation for thermal properties and water content within each soil horizon.

We look for a minimum with respect to *some* parameters in $\mathcal{C}$, followed by a search along other parameters in $\mathcal{C}$ and so on. In details, our approach is formulated in four steps:

1. Select several time intervals $\{\Delta_k\}$ in the period of observations $[0, \tau]$
2. Associate a certain subset $\mathcal{C}_j$ of parameters $\mathcal{C}$ with each Δ_j. The subset $\mathcal{C}_j$ is such that the temperature dynamics over the period Δ_j is primarily determined by

$\mathcal{C}_j$ and depend much less on changes in any other parameters in $\mathcal{C}$.

3. Select a certain pair $\{\Delta_j, \mathcal{C}_j\}$, and look for a location of the minimum of the cost function $J(\mathcal{C})$ keeping all parameters in $\mathcal{C}$ except for $\mathcal{C}_j$ fixed.

4. Update values of $\mathcal{C}_j$ in the control $\mathcal{C}$ by the results obtained at the step (3) and repeat step (3) but for another pair $\{\Delta_i, \mathcal{C}_i\}$, $i \neq j$.

We continue this iterative processes until the difference between the previous and current values of parameters in $\mathcal{C}$ is below a critical tolerance.

The values of t_s and t_e determining lower and upper limits of integration in (10) are equal to the beginning and end of the time interval Δ_k. The choice of Δ_k is naturally dictated by seasons in the hydrological year, which starts at the end of summer and consists of four periods: "winter", "summer and fall", "fall" and "extended summer and fall". Note that the intervals Δ_k can overlap. When the period of observations is one year, typical intervals Δ_k are listed in Table 2. The selected periods Δ_k do not have to coincide with traditional subdivision of a year. For different geographical regions, the timing for the "winter", "summer and fall" and "fall" could be different. Typical timing of periods $\{\Delta_k\}$ for the North Slope of Alaska is shown in Table 2, and are now discussed.

Δ_1 : The "*winter*" period corresponds to the time when the rate of change of the unfrozen liquid water content θ_l is negligibly small; the heat Eq. (2) models the transient heat conduction with thermal properties λ=λ_f, C=C_f, and $\frac{d\theta_l}{dT} \simeq 0$. During the "winter", temperature dynamics depend only on the thermal diffusivity C_f/λ_f of the frozen soil, and hence the simultaneous determination of both parameters C_f and λ_f is an ill-conditioned problem. Assuming that the heat capacity $\{C_f^{(i)}\}$ is known (depending on the soil texture and moisture content we can approximate it using published data), we evaluate the thermal conductivity $\{\lambda_f^{(i)}\}$ and use these values during minimization at other intervals.

Δ_2 : During thawing and freezing periods an active phase change of soil moisture occurs, and hence we consider these periods simultaneously and call their union the

"*summer and fall*", see Table 2. In this time interval, a contribution of the heat capacity C into the apparent heat capacity C_{app} is negligibly small comparing to the contribution of the latent heat term $L d\theta_l/dT$. Therefore, during this interval the rate of freezing/thawing primarily depends on the soil porosity η and the thermal conductivity λ (Tikhonov and Samarskii, 1963). Note that temperature-dependent latent heat effects due to the existence of unfrozen water θ_l at this period have a second order of magnitude effect (see discussion below). Therefore, the coefficients b, T_* parameterizing the unfrozen water content θ_l can be found by taking into account the soil texture and analyzing measured temperature dynamics during the beginning of freeze-up (see Fig. 7). However, we will seek to obtain a better estimates of b, T_* at the next steps, namely during the "fall" period. To summarize the above, we conclude that in the "summer and fall", the temperature dynamics primarily depends on $\{\lambda_t^{(j)}, \eta^{(j)}\}$. Taking into account the relationship (7) between the thermal conductivities for completely frozen and thawed soil, we approximate $\{\lambda_t^{(j)}\}$ for all soil horizons except for the uppermost one by

$$\lambda_t^{(j)} = \lambda_f^{(j)} \left[\frac{\lambda_l}{\lambda_i}\right]^{\eta^{(j)}}, \qquad j = 2, \ldots, n. \tag{26}$$

We remind that the water content $\eta^{(1)}$ in the upper soil horizon is changes over the year due to moisture evaporation and precipitation, and hence formula (26) does not hold for j=1. Hence, during the "summer and fall" period we estimate $\{\eta^{(i)}\}_{i=1}^n$ and $\lambda_t^{(1)}$, and then calculate thermal conductivity $\lambda_t^{(j)}$ for the rest of soil layers j=2, . . . , n by (26).

Δ_3 : Recall that while evaluating the thermal properties $\{\lambda_t^{(i)}, \lambda_f^{(i)}\}$ and the soil porosity $\{\eta^{(i)}\}$, we assumed that the coefficients $\{b^{(i)}, T_*^{(i)}\}$ are known. However they also need to be determined. Also we remind that the coefficients $\{b^{(i)}, T_*^{(i)}\}$ cannot be computed prior to calculation of $\{\lambda_t^{(i)}, \lambda_f^{(i)}\}$ and $\{\eta^{(i)}\}$, since $\{b^{(i)}, T_*^{(i)}\}$ are related to the second order effects in temperature dynamics during "summer and fall" and "winter" intervals.

Once an initial approximation to $\{\lambda_t^{(i)}, \lambda_f^{(i)}\}$ and $\{\eta^{(i)}\}$ is established, we consider the "*fall*" period (see Table 2) during which the temperature dynamics depends mostly on $\{b^{(i)}, T_*^{(i)}\}$ and allows us to capture second order effects in temperature dynamics (Osterkamp and Romanovsky, 1997).

Δ_4 : In the previous three periods, we obtained approximations to all parameters $\{\lambda_t^{(i)}, \lambda_f^{(i)}, C_t^{(i)}, C_f^{(i)}, \eta^{(i)}\}$ and the coefficients $\{b^{(i)}, T_*^{(i)}\}$. We can then improve the approximation by considering the "*extended summer and fall*" period, see Table 2. This period is associated with a time interval when the soil first thaws and then later becomes completely frozen. Since previously, we minimized the cost function depending separately on the porosity $\{\eta^{(i)}\}$ ("summer and fall") and on $\{T_*^{(i)}\}$ ("fall"), we minimize the cost function depending simultaneously on $\{\eta^{(i)}\}$ and $\{T_*^{(i)}\}$ during "extended summer and fall", while other parameters are fixed.

In Table 2, we list all steps and time periods Δ_k which are necessary to find the initial approximation. One of the sequences of minimization steps is

"winter" → "summer and fall" → "fall" → "extended summer and fall"

From our experience with this algorithm, we conclude that in some circumstances it is necessary to repeat minimization over some time periods several times, e.g.

"winter" → "summer and fall" → "fall" → "extended summer and fall" →
"fall" → "extended summer and fall"

until the consecutive iterations modify the thermal properties insignificantly.

6 Multivariate minimization of the cost function

After the selection of the initial approximation, the next step is to minimize the cost function $J(\mathcal{C})$ with respect to all parameters in $\mathcal{C}$. There is a great variety of iterative

methods that minimize $J(\mathcal{C})$. The majority of them rely on computation of the gradient $\nabla J(\mathcal{C})$ of the cost function. The computation of $\nabla J(\mathcal{C})$ is a complicated problem and is out of the scope of this article. An interested reader is referred to (Alifanov et al., 1996; Permyakov, 2004) and to references therein. Since in this article we are primarily concerned with evaluation of the initial approximation to the thermal properties, we use a simplest universal algorithm to minimize the cost function and do not compute the gradients $\nabla J(\mathcal{C})$. However, this algorithm typically converges to the minimum slower than other algorithms that require calculations of the gradient (Dennis and Schnabel, 1987).

7 Application – Happy Valley site

7.1 Short site description

The temperature measurements were taken in the tussock tundra site located at the Happy Valley (69°8′ N ,148°50′ W) in the northern foothills of the Brooks Range in Alaska from 22 July 2001 until 22 February 2005. We used data from 22 July 2001 until 15 May 2002 to estimate soil properties, and from 15 May 2002 until 22 February 2005 to validate the estimated properties. The site was instrumented by eleven thermistors arranged vertically at depths of 0.02, 0.10, 0.17, 0.25, 0.32, 0.40, 0.48, 0.55, 0.70, 0.86 and 1.06 meter. The temperature sensors were embedded into a plastic pipe (the so-called MRC probe), that was inserted into a small diameter hole drilled into the ground. The empty space between the MRC and the ground was filled with a slurry of similar material to diminish an impact of the probe to the thermal regime of soil. Prior to the installation, all sensors were referenced to 0°C in an ice slush bath and have the precision of 0.04°C. An automatic reading of temperature were taken every five minutes, then averaged hourly and stored in a data logger memory.

During the installation, soil horizons were described and their thicknesses were measured. The soil has three distinct horizons: organic cover, organically enriched mineral

soil, and mineral soil. The boundaries between the horizons lie at 0.10 and 0.20 meter depth. Our frost heave measurements show that the vertical displacement of the ground versus the MRC probe is negligibly small at this particular installation site.

In the all following numerical simulations we consider a slab of ground representing the Happy Valley soil between 0.02 and 1.06 meter depth. For the computational purposes, the upper and lower boundary conditions are given by the observed temperatures at depth of 0.02 and 1.06 meter. Also in all computations, the temperatures are compared with the set of measured temperatures at the depths $\{x_i\}$={0.10, 0.17, 0.25, 0.32, 0.40, 0.48, 0.55, 0.70, 0.86} meter.

7.2 Selection of an initial approximation

The *"winter"* period is associated to the ground temperature below −5°C, occurring on 15 January 2002 through 15 May 2002 at the Happy Valley site. The heat capacity C_f for each layer is evaluated based on the soil type, texture and is taken from (Hinzman et al., 1991; Romanovsky and Osterkamp, 1995; Osterkamp and Romanovsky, 1996). We estimate λ_f for each layer by looking for the location of a cost function minimum in the three dimensional space associated with $\lambda_f^{(1)}$, $\lambda_f^{(2)}$ and $\lambda_f^{(3)}$. The minimization problem in this space can be simplified by looking for a minimum in a series of two-dimensional problems as follows. For several physically reasonable realizations of the thermal conductivity $\lambda_f^{(1)}$ (0.25, 0.30, 0.35, . . . , 0.75), we compute temperature dynamics for various values of $\lambda_f^{(2)}$, $\lambda_f^{(3)}$ and plot isolines of the cost function J. From the series of plots in Fig. 8 we can see that the location of the minimum on the $(\lambda_f^{(2)}, \lambda_f^{(3)})$ plane shifts as $\lambda_f^{(1)}$ changes. The minimum of the cost function at each cross section is almost the same, and the problem of selecting the right combination of parameters arises. Here, knowledge of the soil structure becomes relevant. It is known that the soil type of third layer is silt highly enriched with ice, so from Table 1 $1.6<\lambda_f^{(3)}<2.0$. Therefore, we select $\lambda_f^{(1)}$=0.55, $\lambda_f^{(2)}$=1.0 and $\lambda_f^{(3)}$=1.8, and use them in all other consecutive

steps (see Table 3, columns 6, 7 and 8). More precise results could be obtained if a sensor measuring the thermal conductivity was placed in at least one of the horizons (preferably the first one).

In our case, the *"summer and fall"* period is represented by the time interval starting on 28 August 2001 and ending on 6 December 2001. This interval is selected to capture the maximal depth of active layer. Based on the soil type and texture, we assume that $b^{(i)}=-0.7, T_*^{(i)}=-0.03, i=1,2,3$ are a good initial approximation to the coefficients in (3) describing the unfrozen water content (also see Fig. 7). We take values of the heat capacity C_t from (Hinzman et al., 1991; Romanovsky and Osterkamp, 1995; Osterkamp and Romanovsky, 1996). Also, comparing the measured data to temperature dynamics computed for values parameters $\lambda_t^{(1)}$, $\{\eta^{(i)}\}_{i=1}^3$ varying within a range of their natural variability, we found that ranges of these parameters are such that $\lambda_t^{(1)}\in[0.09, 0.15]$, $\eta^{(1)}\in[0.3, 0.9]$, $\eta^{(2)}\in[0.3, 0.9]$ and $\eta^{(3)}\in[0.15, 0.45]$. Once, the ranges of the parameters are established, we can look for a minimum of the cost function in the four dimensional space associated with $\lambda_t^{(1)}, \{\eta^{(i)}\}_{i=1}^3$. We stress again that it is unnecessary to find the minimum in this space very accurately but rather only to estimate its location as significant uncertainties in other parameters still exist.

An approximate solution of the four dimensional minimization problem can be found, for instance, by evaluating the cost function on $(\lambda_t^{(1)}, \eta^{(1)})$, $(\eta^{(1)}, \eta^{(2)})$ and $(\eta^{(2)}, \eta^{(3)})$ planes as follows. We set $\eta^{(1)}=0.6$, $\eta^{(2)}=0.6$, $\eta^{(3)}=0.3$ and $\lambda_t^{(1)}=0.12$, which correspond to the middle of their variability ranges. Recall that from minimizing over the "winter" interval we obtained $\lambda_f^{(1)}=0.55$, $\lambda_f^{(2)}=1.0$ and $\lambda_f^{(3)}=1.8$. The first approximation to other parameters in control are also known: $b^{(i)}=-0.7$ and $T_*^{(i)}=-0.03$ are the initial approximation; $\lambda_t^{(i)}$ for $i=2,3$ are computed by Formula (26). Therefore, to evaluate the cost function on the $(\lambda_t^{(1)}, \eta^{(1)})$ plane, we vary the parameters $\lambda_t^{(1)}, \eta^{(1)}$ in the control, while the other parameters are fixed ($\eta^{(2)}=0.6$, $\eta^{(3)}=0.3$ just for this plane, see Table 3, "Summer and Fall" 1st row for values of the rest of parameters). After evaluating the

cost functions on all three planes, we look for its minima (see Fig. 9, left). At the $(\lambda_t^{(1)}, \eta^{(1)})$ plane, the cost function attains its minimal value on a boundary of this plane, see Fig. 9, upper left, and is minimal in the center of the planes $(\eta^{(1)}, \eta^{(2)})$, $(\eta^{(2)}, \eta^{(3)})$. The last two planes allows us to find that $\eta^{(1)}$=0.6, $\eta^{(2)}$=0.55 and $\eta^{(3)}$=0.27, whereas contours at the first plane show that the value of $\lambda_t^{(1)}$ lies between 0.11 and 0.13, see Fig. 9, left column. We suppose that $\lambda_t^{(1)}$ is 0.12 and proceed further. After updating the control with the computed values, we evaluate the cost function on the same set of planes one more time; parameters in the control before minimization are shown in Table 3 the "Summer and Fall" 2^{nd} row. After computing the cost function, we draw its isolines and show them in Fig. 9, right. Note that at this step the cost function attains its minima located in the center of the computational grid. We update the control with $\eta^{(1)}$=0.6, $\eta^{(2)}$=0.55, $\eta^{(3)}$=0.27, $\lambda_t^{(1)}$=0.12. Note that the location of the minimum did not change significantly. Our experience shows that the change of soil properties by 10% or less is considered to be insignificant, since the difference between soil temperatures computed with and without changes in parameters is typically comparable with uncertainties of measurements. Finally, we do not need to complete additional iterations on the same set of planes, since there are still uncertainties in other parameters. We use the updated parameters and proceed to the next step, the evaluation of coefficients T_* and b.

The *"fall"* period is represented by a time interval which begins when the soil starts to freeze and ends when the temperature becomes near −5°C. In our case this period begins on 27 October 2001 and ends on 5 January 2002. We recall that from minimizations at previous intervals ("winter", "summer and fall"), we obtained that $\lambda_f^{(1)}$=0.55, $\lambda_f^{(2)}$=1.0, and $\lambda_f^{(3)}$=1.8; $\lambda_t^{(1)}$=0.12, $\eta^{(1)}$=0.6, $\eta^{(2)}$=0.55, and $\eta^{(3)}$=0.27, see Table 3, the "Fall" 1^{st} row. However, to derive these values we used an approximation to the coefficients parameterizing the unfrozen water content, namely $b^{(i)}$=−0.7 and $T_*^{(i)}$=−0.03 for i=1, 2, 3. To compute better approximations to $\{b^{(i)}\}$ and $\{T_*^{(i)}\}$, we minimize the

cost function with respect to $\{b^{(i)}, T_*^{(i)}\}_{i=1}^3$ during the "fall" interval using approximate values of the thermal conductivity $\{\lambda_f^{(i)}\}_{i=1}^3$ and porosity $\{\eta^{(i)}\}_{i=1}^3$ from previous results. Since we need an approximate solution to the minimization problem, we look for the minimum of J in the $(T_*^{(1)}, b^{(1)})$, $(T_*^{(2)}, b^{(2)})$ and $(T_*^{(3)}, b^{(3)})$ planes[1] (see Fig. 10, left). For example, to compute the cost function on the $(T_*^{(1)}, b^{(1)})$ plane, we vary the values of $T_*^{(1)}, b^{(1)}$ in the control while other parameters are fixed. We remind that the thermal properties are obtained in the "winter" and "summer and fall", and $T_*^{(2)}=T_*^{(3)}=-0.03$ and $b^{(2)}=b^{(3)}=-0.7$ is the assumed approximation. Computations associated with other planes are completed similarly, with fixed parameters set equal to their previously used values. After finding minima, we update the control accordingly to $b^{(1)}=-0.7$, $b^{(2)}=-0.6$, $b^{(3)}=-0.75$ and $T_*^{(1)}=-0.03$, $T_*^{(2)}=-0.03$ and $T_*^{(3)}=-0.03$. After updating the control (see Table 3, the "Fall" 2^{nd} row), we minimize the cost function on the same sets of planes one more time and obtain that a new set of minima corresponding to $b^{(1)}=-0.7$, $b^{(3)}=-0.75$ and $T_*^{(1)}=-0.03$, $T_*^{(3)}=-0.03$, see Fig. 10 right. However, on the plane $(T_*^{(2)}, b^{(2)})$, the minimum is attended on the boundary of the region. Therefore, we exploit the previous values of the coefficients $b^{(2)}, T_*^{(2)}$, namely $b^{(2)}=-0.6$, $T_*^{(2)}=-0.03$, and have to consider some additional iterations. These additional iterations are associated with the "extended summer and fall" period.

From previous minimizations, we evaluated approximation to all unknown parameters in the control, i.e. $\lambda_t^{(1)} = 0.12$, $\eta^{(1)}=0.6$, $\eta^{(2)} = 0.55$, $\eta^{(3)}=0.27$ and $b^{(1)}=-0.65$, $b^{(2)}=-0.6$, $b^{(3)}=-0.75$ and $T_*^{(1)}=-0.02$, $T_*^{(2)}=-0.03$, $T_*^{(3)}=-0.03$, see Table 3, the Extended Summer and Fall 1^{st} row. However, we can improve the quality of our ap-

[1]Other selection of planes is possible. We emphasize that we are just interested in calculation of an initial approximation to the control which could serve as a starting point in the global minimization of the cost function. By no means, do we try to substitute the global minimization by this heuristic procedure. However, a good starting point can save computational time and improve accuracy of a final result.

proximation by repeating minimization processes associated with the "summer and fall" and "fall" intervals, or by considering the "*extended summer and fall*" period. In our case, this period begins on 28 August 2001 when the active layers is developed and ends when temperature becomes less than $-5^{\circ}C$ on 5 January 2002. During these period we look for the minimum of the cost function with respect to six parameters $\{\eta^{(i)}, T_*^{(i)}\}_{i=1}^{3}$. We propose to select the set of planes $(T_*^{(1)}, \eta^{(1)})$, $(T_*^{(2)}, \eta^{(2)})$ and $(T_*^{(3)}, \eta^{(3)})$, and minimize the cost function only over them. After the first step, we find that the minimum is located at $\eta^{(1)}$=0.7, $\eta^{(2)}$=0.55, $\eta^{(3)}$=0.27 and $T_*^{(1)}$=−0.025, $T_*^{(2)}$=−0.03, $T_*^{(3)}$=−0.03, see Fig. 11 left. After updating the parameters in the control, we look for a minimum of the cost function on the same sets of planes another time in order to check that the minima are coincident. We obtain that $\eta^{(1)}$=0.7, $\eta^{(2)}$=0.55, $\eta^{(3)}$=0.27 and $T_*^{(1)}$=−0.025, $T_*^{(2)}$=−0.025, $T_*^{(3)}$=−0.03, see Fig. 11 right. Since locations of the minima did not change significantly between the last two minimizations, we assume that we converged to some minimum.

7.3 Global minimization and sensitivity analysis

While evaluating an initial approximation, we sought minimums of the cost functions $J(\mathcal{C})$ measuring discrepancy over periods $\{\Delta_k\}$. In this subsection, we perform global minimization of the cost function with respect to all parameters in $\mathcal{C}$ over the entire period of measurements 22 July 2001 until 15 May 2002 used for calibration. Also, we analyze sensitivity of an initial approximation derived from minimizing the cost function globally with respect to all parameters.

In global minimization problems, a starting point from which iterations begin is given by the initial approximation evaluated in the previous subsection, see Table 3, the last row. In our study we try to look for the minimum of the cost function by the simplex search method described in (Lagarias et al., 1998), which is a direct search method (Bazaraa et al., 1993). In a two and three dimensional spaces, the simplex is a triangle or a pyramid, respectively. At each iteration the value of the function computed at the

point, being in or near the current simplex, is compared with the function's values at the vertices of the simplex and, usually, one of the vertices is replaced by the new point, giving a new simplex. The iteration processes is continued until the simplex sizes are less than an a priori specified tolerance. At the final iteration, we obtain the set of parameters that determine the thermal properties, porosity and coefficients specifying the unfrozen water content for each soil horizon.

It is important to notice that the set of parameters we obtain as a result of global minimization problem can depend on values t_s and t_e determining the period over which discrepancy between observed and modeled temperatures is measured. In global minimization problems, the constant t_e is associated with an end of "winter" interval during which the soil is completely frozen. But since, the soil is frozen for several months for a cold permafrost region, the cost function does not significantly depends on t_e if t_e varies within two week limits. However, the value of t_s is associated with beginning of "summer and fall" interval during which the ground is thawed. Since, the ground is thawing during a relatively short period of time for cold permafrost regions, we consider several values of t_s and minimize the cost function with respect to all parameters.

Results of minimization are listed in Table 4. It shows that the initial approximations do not significantly depend on constants t_s, if the interval $[t_s, t_e]$ represents thawed and frozen states of the soil. Using averaged values of the thermal properties, we compute the temperature dynamics for the entire period of observations. Comparison of the calculated and measured temperatures at different depths and at time intervals used for calibration are shown in Figs. 12, 13 and 14. During the winter, the calculated temperature closely follows the observed temperature within the uncertainty of thermistor measurements. During the summer, the difference between the measured and calculated temperatures is larger but does not exceed 0.3°C for sensors in the mineral soil. This larger discrepancy between the measured and computed temperatures can be partially explained by over-simplifying physics and neglecting water dynamics in the upper organic horizons.

Finally, in order to show that the found initial approximation (the last row in Table 3)

lies close to the true values of soil properties, we use it to compute the soil temperature dynamics through 22 February 2005. Note that the time interval from 22 May 2002 until 22 February 2005 was not used to find the initial approximation. In Fig. 15, we plot the measured and calculated temperature dynamics at 0.40 and 0.70 meter depths. The difference between the calculated and measured temperature dynamics is typically less than 0.25°C, however during the summer it is higher. One of the explanations that the measured temperatures are higher than the computed ones is that the MRC probe slightly heaves, and the temperature sensors which was at 0.40 meter depth initially on 22 July 2001 is located several centimeters higher on 22 February 2005.

8 Discussion and limitation of the proposed method

In this paper we described one of the approaches that can be used to find an initial approximation to the thermal properties of soil horizons. This technique approximates the thermal conductivity, porosity, unfrozen water content curve in horizons where no direct temperature measurements are available. We admit that we find only one of the possible initial approximations, which can be utilized as the so-called initial educated guess in a multivariate minimization problem. However, during evaluation of the initial approximation, we derive multiple limiting boundaries on parameters which can serve as constrains during multivariate minimization and hence produce reasonable estimates of the thermal properties.

One of the limitations of the proposed approach is that it requires values of heat capacities, since at certain time periods it is possible to estimate thermal diffusivity only but not thermal conductivity and heat capacity separately.

It should be noted that recovery of the thermal properties of the organic cover (e.g. moss layer) is given as an integrated approach in the following sense. Complex physical processes occurring in the organic cover that include non-conductive heat transfer (Kane et al., 2001) are taken into account by estimating some effective thermal properties which are constants for the entire season. We acknowledge that

the estimated thermal properties of the organic layer could be different in nature, but we recover them in such a way that the temperature in the active layer and permafrost should correspond to the measured one.

In the proposed model we used 1-D assumption regarding the heat diffusion in the active layer, which sometimes is not applicable due to hummocky terrain in the Arctic tundra. Another assumption used in the model is that frost heave and thaw settlement is negligibly small and there is no ice lens formation in the ground during freezing. Therefore, the proposed method could be only applied where these assumption are satisfied.

The proposed method allows computation of a volumetric content η of water which changes its phase during freezing or thawing. Water content of liquid water that is tightly bound to soil particles and is not changing its phase can not be estimated within the proposed model (2).

9 Conclusions

We developed an approach to calculate an approximation to soil porosity and thermal properties in order to use it as the initial guess in commonly exploiting data assimilation techniques. To compute the approximation, we minimize the multivariate cost function describing discrepancy between the measured and calculated temperatures over a certain time interval. We find the minimum by adopting a coordinate-wise iterative search technique to the specifics of our inverse problem. At each iteration, we select a particular set of soil properties and associate with them a certain time interval over which we minimize the cost function. After employing the proposed sequence of iterations, it is possible to find the approximation to all thermal properties and soil porosity.

Although there are several limitations to the proposed approach, we applied it to recover soil properties for Happy Valley site near Dalton highway in Alaska. The difference between the simulated and measured temperature dynamics over the periods of

calibration is typically less than 0.3°C. The difference between the simulated and measured temperatures over the consecutive time interval not used in calibration is less than 0.5°C which shows a good agreement with measurements, and validates that the found initial approximation lies close to the true values of soil properties.

In order to compute the cost function, it is necessary to calculate the soil temperature dynamics. Therefore, we developed a new finite element discretization of the Stefan-type problem on fixed coarse grids using enthalpy formulation. One of the advantages of the new method is that it allows computation of the temperature dynamics for the classical Stefan problem without any smoothing of the enthalpy. Also, new approach shows equal or better performance comparing to other finite element models of the ground thawing and freezing processes.

Acknowledgements. We would like to thank J. Straw, S. Marchenko and P. Layer for all their advice, critique and reassurances along the way. This research was funded by ARCSS Program and by the Polar Earth Science Program, Office of Polar Programs, National Science Foundation (OPP-0120736, ARC-0632400, ARC-0520578, ARC-0612533, IARC-NSF CA: Project 3.1 Permafrost Research), by NASA Water and Energy Cycle grant, and by the State of Alaska.

References

ACIA: Impacts of a Warming Arctic: Arctic Climate Impact Assessment, Cambridge University Press, 139pp, 2004. 214

Alifanov, O.: Inverse Heat Transfer Problems, Springer, Berlin, 1994. 222

Alifanov, O., Artyukhin, E., and Rumyantsev, S.: Extreme Methods for Solving Ill-Posed Problems with Application to Inverse Heat Transfer Problems, Begell House, New York, 1996. 221, 222, 236

Andersland, O. and Anderson, D.: Geotechnical Engineering for Cold Regions, McGraw-Hill, 1978. 215

Anderson, D. and Morgenstern, N.: Physics, chemistry and mechanics of frozen ground: A review, in: Proceedings Second International Conference on Permafrost, 257–288, Yakutsk, USSR, 1973. 217

Avriel, M.: Nonlinear Programming: Analysis and Methods, Dover Publications, 2003. 216
Bazaraa, M., Sherali, H., and Shetty, C. M.: Nonlinear Programming: Theory and Algorithms, John Wiley & Sons, 2nd edn., 1993. 232, 241
Boike, J. and Roth, K.: Time Domain Re?ectometry as a Field Method for Measuring Water Content and Soil Water Electrical Conductivity at a Continuous Permafrost Site, Permafrost and Periglacial Processes, 8, 359–370, 1997. 220
Brown, J., Ferrians, O., Heginbottom, J. J., and Melnikov, E.: Circum-Arctic map of permafrost and ground-ice conditions, U.S. Geological Survey Circum-Pacific Map CP-45, 1:10 000 000, reston, Virginia, 1997. 214
Carslaw, H. and Jaeger, J.: Conduction of heat in solids, Oxford Univ. Press, London, 1959. 217
Carson, J.: Analysis of soil and air temperatures by Fourier techniques, Journal Geophysical Research, 68, 2217–2232, 1963. 221
Comini, G., Giudice, S. D., Lewis, R., and Zienkiewicz, O.: Finite element solution of non-linear heat conduction problems with special reference to phase change, Int. J. Numer. Methods Engng, 8, 613–624, 1974. 225
Dalhuijsen, A. and Segal, A.: Comparison of finite element techniques for solidification problems, Int.j .numer.methods eng., 23, 1807–1829, 1986. 231
Dennis, J. and Schnabel, R.: Numerical Methods for Unconstrained Optimization and Nonlinear Equations, Prentice-Hall, 1987. 236
de Vries, D.: W. R. van Wijk (editor) Physics of the plant environment, chap. Thermal Properties of Soils, North-Holland, Amsterdam, 1963. 218
Fletcher, R.: Practical methods of optimization, John Wiley & Sons, 2000. 223
Goodrich, W.: The influence of snow cover on the ground thermal regime, Candian Geotechnical Journal, 19, 1982. 215
Gupta, S.: The Classical Stefan Problem, Elsevier, Amsterdam, 2003. 221, 230
Hinkel, K. M.: Estimating seasonal values of thermal diffusivity in thawed and frozen soils using temperature time series, Cold Reg. Sci. Technol., 26, 1–15, 1997. 221
Hinzman, L., Kane, D., Gleck, R., and Everett, K.: Hydrological and thermal properties of the active layer in the Alsakan Arctic, Cold Region Science and Technology, 19, 95–110, 1991. 219, 237, 238
Hobbs, P.: Ice physics, Claredon Press, Oxford, 1974. 217, 218
Hurley, S. and Wiltshire, R. J.: Computing thermal diffusivity from soil temperature measure-

ments, Comput. Geosci., 19, 475–477, 1993. 221
Jaeger, J. C. and Sass, J. H.: A line source method for measuring the thermal conductivity and diffusivity of cylindrical specimens of rock and other poor conductors, J. Appl. Phys., 15, 1187–1194, 1964. 220
Javierre, E., Vuik, C., Vermolen, F., and van der Zwaag, S.: A comparison of numerical models for one-dimensional Stefan problems, Journal of Computational and Applied Mathematics, 192, 445–459, 2006. 224
Kane, D., Hinzman, L., and Zarling, J.: Thermal response of the active layer in a permafrost environment to climatic warming, Cold Region Science Technology, 19, 111–122, 1991. 215
Kane, D., Hinkel, K., Goering, D., Hinzman, L., and Outcalt, S.: Non-conductive Heat Transfer Associated with Frozen Soils, Global and Planetary Change, 29, 275–292, 2001. 219, 243
Lagarias, J., Reeds, J., Wright, M., and Wright, P.: Convergence Properties of the Nelder-Mead Simplex Method in Low Dimension, SIAM Journal of Optimization, 9, 112–147, 1998. 241
Lemmon, E.: R.W. Lewis and K. Morgan (ed.), Numerical Methods in Thermal Problems, chap. Phase change technique for finite element conduction code, pp. 149–158, Pineridge Press, Swansea, U.K., 1979. 225
Ling, F. and Zhang, T.: Impact of the timing and duration of seasonal snow cover on the active layer and permafrost in the Alaskan Arctic, Permafrost Periglacial Processes, 14, 141–150, 2003. 215
Lovell, C.: Temperature effects on phase composition and strength of partially frozen soil, Highway Res. Board Bull., 168, 74–95, 1957. 218
McGaw, R. W., Outcalt, S. I., and Ng, E.: Thermal properties of wet tundra soils at Barrow, Alaska, Proceedings of 3rd International Conference on Permafrost, 1, 47–53, nat. Res. Counc. of Can., Ottawa,Canada, 1978. 221
Molders, N. and Romanovsky, V.: Long-term evaluation of HTSVS frozen ground/permafrost component using observations at Barrow, Alaska., J. Geophys. Res., 111, doi:10.1029/2005JD005957, 2006. 215
Morgan, K., Lewis, R., and Zienkiewicz, O.: An improved algorithm for heat conduction problems with phase change, Int. j .numer.methods eng., 12, 1191–1195, 1978. 225
Mundim, M. and Fortes, M.: edited by: Numerical Methods in Thermal Problems, edited by: Lewis, R. W. and Morgan, K., vol. 6, chap. Evaluation of finite element method utilised in the solution of solid-liquid phase change problems, pp. 90–100, Pineridge Press, Swansea, U.K., 1979. 226

Muzylev, N. V.: The uniqueness of a solution to an inverse nonlinear heat conduction problem, Zhurnal Vychislitel'noi Matematiki i Matematicheskoi Fiziki, 25, 1346–1352, in Russian, 1985. 224
Nelson, F. and Outcalt, S.: Anthropogenic geomorphology in northern Alaska, Physical Geography, 3, 17–48, 1987. 215
Oleson, K. W., Dai, Y., Bonan, G., Bosilovich, M., Dickinson, R., Dirmeyer, P., Hoffman, F., Houser, P., Levis, S., Niu, G.-Y., Thornton, P., Vertenstein, M., Yang, Z.-L., and Zeng, X.: Technical description of the Community Land Model (CLM), NCAR tech. note NCAR/TN-461+STR, NCAR, 2004. 215
Osterkamp, T. and Romanovsky, V.: Characteristics of changing permafrost termperatures in the Alaskan Arctic, USA, Arctic and Alpine research, 28, 267–273, 1996. 237, 238
Osterkamp, T. and Romanovsky, V.: Freezing of the active layer on the Coastal Plain of the Alaskan Arctic, Permafrost and Periglacial Processes, 8, 23–44, 1997. 217, 235
Permyakov, P.: Methods of Determining the Characteristics of Dispersed Media at a Phase Transition, Russian Physics Journal, 2004. 236
Pham, Q. T.: Comparison of general-purpose finite element methods for the Stefan problem, Numerical Heat Transfer Part B - Fundamentals, 27, 417–435, 1995. 225
Pinder, G. and Gray, W.: Finite Element Simulation in Surface and Subsurface Hydrology, Academic Press, New York, 1977. 231, 232
Rank, E., Katz, C., and Werner, H.: On the importance of the discrete maximum principle in transient analysis using finite element methods, Int. j .numer.methods eng., 19, 1771–1782, 1983. 231
Romanovsky, V. and Osterkamp, T.: Interannual variations of the thermal regime of the active layer and near-surface permafrost in Northern Alaska, Permafrost and Periglacial Processes, 6, 313–335, 1995. 237, 238
Romanovsky, V. and Osterkamp, T.: Thawing of the Active Layer on the Coastal Plain of the Alaskan Arctic, Permafrost and Periglacial processes, 8, 1–22, 1997. 219
Samarskii, A. and Vabishchevich, P.: Computational Heat Transfer, Mathematical Modelling, vol. 1,2, Wiley, first edn., 1996. 221
Sass, J., Lachenbruch, A., and Munroe, R.: Thermal conductivity of rocks from measurements on fragments and its application to heat-flow determinations, J. Geophys. Res., 76, 3391–3401, 1971. 218
Sazonova, T., Romanovsky, V., Walsh, J., and Sergueev, D.: Permafrost dynamics in the

20th and 21st centuries along the East Siberian transect, J. Geophys. Res., 109, D01108, doi:10.1029/2003JD003680, 2004. 215
Schmugge, T., Jackson, T., and McKim, H.: Survey of Methods for Soil Moisture Determination, Water Resour. Res., 16, 961–979, 1980. 220
Smith, M. and Tice, A.: Measurement of the unfrozen water content of soilscomparison of NMR and TDR methods, CRREL Report 88–18, US Army Cold Regions Research and Engineering Lab (CRREL), 1988. 220
Stafford, J.: REMOTE, NON-CONTACT AND IN-SITU MEASUREMENT OF SOIL MOISTURE CONTENT: A REVIEW, The Journal of Agricultural Engineering Research, pp. 151–172, 1988. 220
Thacker, W.: The role of the Hessian matrix in fitting models to measurements, Journal of Geophysical Research, 94, 6177–6196, 1989. 224
Thacker, W. and Long, R.: Fitting dynamics to data, J. Geophys. Res., 93, 1227–1240, 1988. 216
Tice, A., Oliphant, J., Nakano, Y., and Jenkins, T.: Relationship between the ice and unfrozen water phases in frozen soil as determined by pulsed nuclear magnetic resonance and physical desorption data, CRREL Report 82–15, US Army Cold Regions Research and Engineering Lab (CRREL), 1982. 220
Tikhonov, A. and Samarskii, A.: Equations of mathematical physics, Pergamon, 1963. 234
Tikhonov, L. and Leonov, A.: Nonlinear Ill-Posed Problems, vol. 14 of *Applied Mathematics and Mathematical Computation Series*, Chapman and Hall, London, 1996. 222
Topp, G. C., Davis, J. L., and Annan, A. P.: Electromagnetic determination of soil water content: measurements in coaxial transmission lines, Water Resour. Res., 16, 574–582, 1980. 220
Ulaby, F., Moore, R., and Fung, A.: Microwave Remote Sensing, Addison-Wesley, Reading, MA, 1982. 220
Voller, V. and Swaminathan, C.: Fixed grid techniques for phase change problems: a review, Int.j .numer.methods eng., 30, 875–898, 1990. 225
Watanabe, K. and Mizoguchi, M.: Amount of unfrozen water in frozen porous media saturated with solution, Cold Regions Science and Technology, 34, 103–110, 2002. 217
Williams, P.: Properties and behaviour of freezing soils, Tech. Rep. 72, Norwegian Geotechnical Institute, 1967. 217
Yershov, E.: General Geocryology, Cambridge University Press, New York, 1998. 215
Yoshikawa, K., Overduin1, P., and Harden, J.: Moisture Content Measurements of Moss

(Sphagnum spp.) using Commercial Sensors, Permafrost and Periglacial Processes, 15, 309-318, 2004. 215, 220

Zhang, T. and Osterkamp, T. E.: Considerations in determining the thermal diffusivity from temperature time series using finite difference methods, Cold Reg. Sci. Technol., 23, 333–341, 1995. 215, 221

Zhuang, Q., Romanovsky, V., and McGuire, A.: Incorporation of a permafrost model into a large-scale ecosystem model: Evaluation of temporal and spatial scaling issues in simulating soil thermal dynamics, Journal Geophysical Research, 106, 33 649–33 670, 2001. 215

Zienkiewicz, O. and Taylor, R.: The finite element method, vol. 1,2, McGraw-Hill, London, fourth edn., 1991. 221, 227, 230

Table 1. A typical thickness of soil layers and commonly occurring range of thermal properties in a cryosol soil at the North Slope, Alaska.

Layer	Layer thickness	Thermal conductivity in the frozen state, λ_f	Porosity, η	Coefficient in (3) b
Moss or organic layer	0.05	[0.1, 0.5]	[0.1, 0.7]	[−1, −0.5]
Mineral-organic mixture	0.20	[0.7, 1.5]	[0.2, 0.6]	[−0.8, −0.5]
Mineral soil	> 1.0	[1.3, 2.4]	[0.2, 0.4]	[−0.7, −0.5]

Table 2. Typical choice of parameters in the control $\mathcal{C}$ for "cold" permafrost regions.

Periods	$\mathcal{C}_j$	Typical Δ_k	Characteristic	Step
"Winter"	$\{\lambda_f^{(i)}\}$	December–April	Completely frozen ground, $T<-5^{\circ}$C	1
"Summer and Fall"	$\{\eta^{(i)}\},\lambda_t^{(1)}$	May–November	Developing/-ed active layer and its freezing	2
"Fall"	$\{b^{(i)}, T_*^{(i)}\}$	September–December	Active layer freezing, $T>-5^{\circ}$C	3
"Extended Summer and Fall"	$\{\eta^{(i)}, T_*^{(i)}\}$	May–January	Developing/-ed active layer and its freezing	4

Table 3. Values of the parameters in the control at the beginning of each minimization step. The parameters which values are in the parenthesis with the same subindex define minimization plane. For example, in the third row $\lambda_t^{(1)}$ and $\eta^{(1)}$ are in the parenthesis and have the same subindex equal to 1. Therefore, this pair define a minimization plane $(\lambda_t^{(1)}, \eta^{(1)})$. On this plane we minimize the cost function depending on $\lambda_t^{(1)}$ and $\eta^{(1)}$, while value of other parameters are fixed and given in other sections of the current row.

Iterations	$\eta^{(1)}$	$\eta^{(2)}$	$\eta^{(3)}$	$\lambda_t^{(1)}$	$\lambda_f^{(1)}$	$\lambda_f^{(2)}$	$\lambda_f^{(3)}$	$b^{(1)}$	$b^{(2)}$	$b^{(3)}$	$T_*^{(1)}$	$T_*^{(2)}$	$T_*^{(3)}$
Winter	0.40	0.70	0.25	0.10	–	–	–	−0.7	−0.7	−0.7	−0.03	−0.03	−0.03
Summer and Fall, 1st	$(0.60)_{1,2}$	$(0.60)_{2,3}$	$(0.30)_3$	$(0.12)_1$	0.55	1.00	1.80	−0.7	−0.7	−0.7	−0.03	−0.03	−0.03
Summer and Fall, 2nd	$(0.60)_1$	$(0.55)_{1,2}$	$(0.27)_{2,3}$	$(0.12)_3$	0.55	1.00	1.80	−0.7	−0.7	−0.7	−0.03	−0.03	−0.03
Fall, 1st	0.60	0.55	0.27	0.12	0.55	1.00	1.80	$(-0.7)_1$	$(-0.7)_2$	$(-0.7)_3$	$(-0.03)_1$	$(-0.03)_2$	$(-0.03)_3$
Fall, 2nd	0.60	0.55	0.27	0.12	0.55	1.00	1.80	$(-0.7)_1$	$(-0.6)_2$	$(-0.75)_3$	$(-0.03)_1$	$(-0.03)_2$	$(-0.03)_3$
Ext. Summer and Fall 1^{st}	$(0.60)_1$	$(0.55)_2$	$(0.27)_3$	0.12	0.55	1.00	1.80	−0.65	−0.6	−0.75	$(-0.02)_1$	$(-0.03)_2$	$(-0.03)_3$
Ext. Summer and Fall 2^{nd}	$(0.70)_1$	$(0.55)_2$	$(0.27)_3$	0.12	0.55	1.00	1.80	−0.65	−0.6	−0.75	$(-0.025)_1$	$(-0.03)_2$	$(-0.03)_3$
Final Result	0.70	0.55	0.27	0.12	0.55	1.00	1.80	−0.65	−0.6	−0.75	−0.025	−0.025	−0.03

Table 4. Global minimization with respect to all parameters in the control. Each realization is specified by the time interval $[t_s, t_e]$ over which the discrepancy between the data and computed temperature dynamics is evaluated. In all case, the constant t_e is associated to the ...

t_s	$\eta^{(1)}$	$\eta^{(2)}$	$\eta^{(3)}$	$\lambda_t^{(1)}$	$\lambda_f^{(1)}$	$\lambda_f^{(2)}$	$\lambda_f^{(3)}$	$b^{(1)}$	$b^{(2)}$	$b^{(3)}$	$T_*^{(1)}$	$T_*^{(2)}$	$T_*^{(3)}$
18 August	0.703	0.560	0.272	0.120	0.562	0.983	1.797	−0.655	−0.596	−0.750	−0.0251	−0.0253	−0.0301
22 August	0.721	0.557	0.272	0.122	0.559	0.973	1.809	−0.673	−0.558	−0.757	−0.0256	−0.0249	−0.0295
26 August	0.718	0.546	0.272	0.122	0.559	0.962	1.801	−0.657	−0.597	−0.755	−0.0250	−0.0251	−0.0303
30 August	0.712	0.549	0.272	0.121	0.556	0.967	1.801	−0.655	−0.601	−0.755	−0.0251	−0.0251	−0.0302
3 September	0.712	0.544	0.274	0.123	0.559	0.980	1.816	−0.665	−0.551	−0.750	−0.0255	−0.0255	−0.0298
7 September	0.718	0.534	0.274	0.123	0.560	0.966	1.789	−0.660	−0.603	−0.747	−0.0250	−0.0252	−0.0297

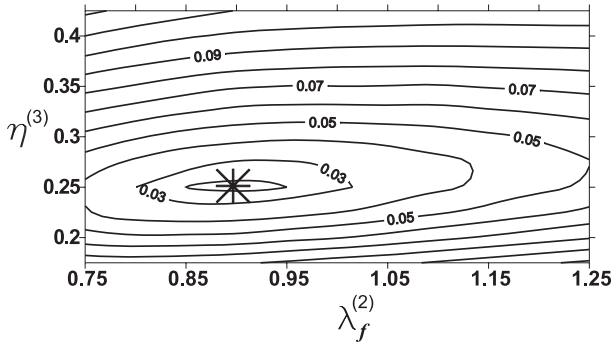

Fig. 1. Isolines of the cost function $J(\mathcal{C})$ computed using the synthetic temperature data T_S. The minimum of the cost function is marked by the start and is located at $\lambda_f^{(2)}$=0.9 and $\eta^{(3)}$=0.25, which is coincide with the values of $\lambda_f^{(2)}$, $\eta^{(3)}$ used to compute T_S.

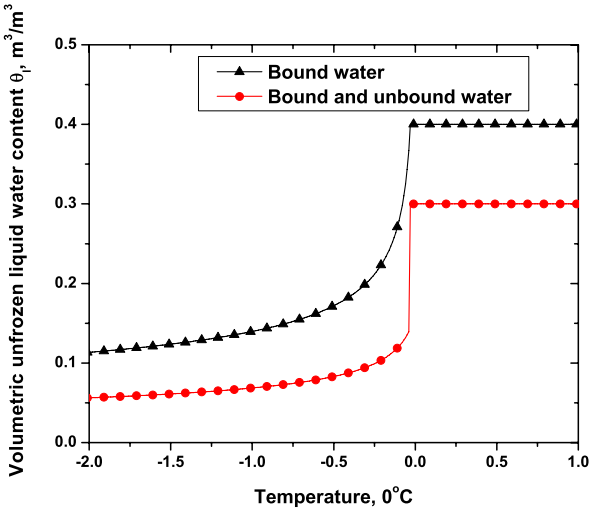

Fig. 2. Typical volumetric content of the unfrozen liquid water in soils as a function of temperature. The curve marked by triangles is associated with soils in which all water is bound in soil pores, and hence the water content gradually decreases with decreasing temperature in °C. The curve marked by circles is related to soils in which some percentage of water is not bound to the soil particle and changes its phase at the temperature T_*, while other part of liquid water is bound in soil pores and freezes gradually as the temperature decreases.

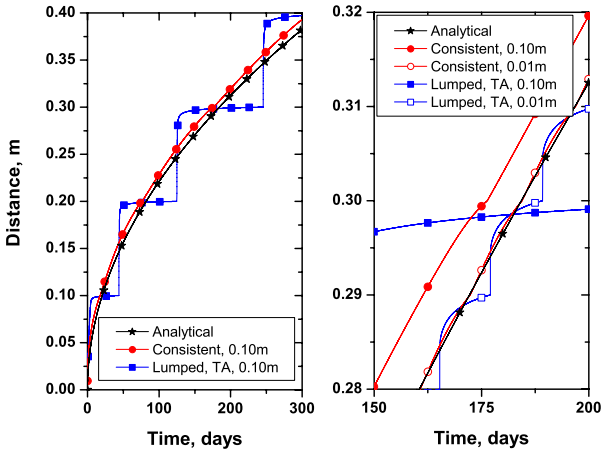

Fig. 3. Comparison of analytical (stars) and numerical solutions. Initially, the soil has −5°C temperature, and at the time t=0, the temperature at its upper boundary is changed to 1°C. At the lower boundary located at 5 meter depth, zero flux boundary condition is specified. On the left plot, we show a location of the 0°C isotherm calculated for a uniform spatial discretizations with 0.1 m grid element. The numerical solutions are computed by the proposed method (circles) and by the scheme using the lumped approach with temporal enthalpy averaging (squares). On the right plot, we show a location of the 0°C isotherm calculated for a uniform spatial discretizations with 0.1 m (filled) and 0.01 m (hollow) grid elements.

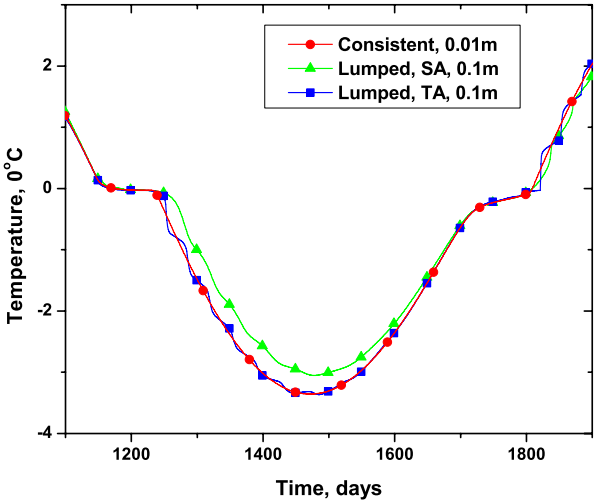

Fig. 4. Temperature dynamics at 0.3 meter depth computed by the consistent (circles) and mass lumped approaches (squares, triangles). The temperatures marked by squares and triangles are calculated by mass lumped approach with temporal (squares, TA) and spatial (triangles, SA) enthalpy averaging and with a uniform 0.1 m spatial discretization. The temperature computed by the consistent approach (circles) was evaluated on a uniform grid with 0.01 m elements. Initially the temperature is zero, the upper boundary condition is given by Dirichlet type boundary condition with a slowly varying sinusoid having the amplitude of 3°C and the period of there years; zero heat flux is specified at 2 meter depth.

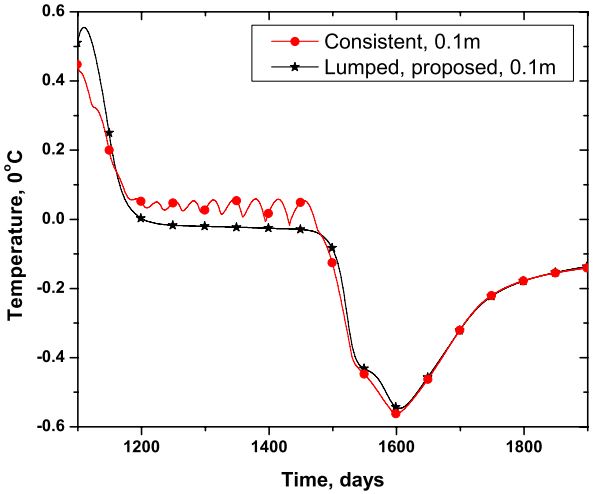

Fig. 5. Temperature dynamics at 1 meter depth computed by the proposed consistent (circles) and the mass lumped schemes (stars). The mass lumped scheme is based on (25). In order to emphasis numerical oscillations occurring in the case of small time steps in the consistent approach, we use a uniform grid with 0.1 m grid elements. The oscillations are due to violation of the discrete maximum principle in the consistent scheme during active phase change processes. The initial and boundary conditions are the same as stated in caption of Fig. 4.

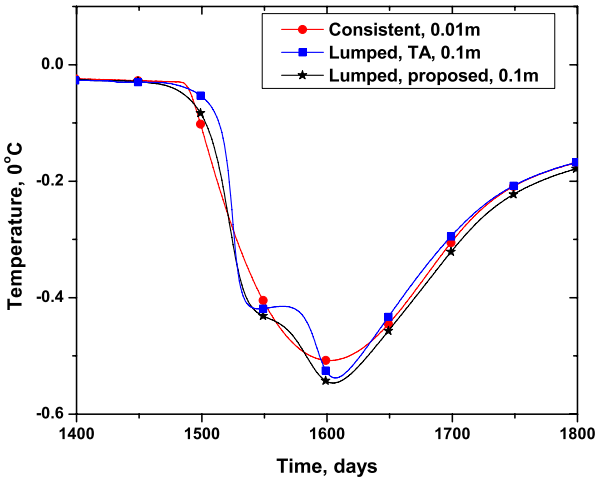

Fig. 6. Temperature dynamics at 1 meter depth computed by the consistent approach (circles), the proposed mass lumped approach (stars) and the mass lumped approach with temporal enthalpy averaging (squares). The temperatures computed mass lumped approach are found on uniform grid with 0.1 m grid elements, whereas in the consistent approach, the length of grid elements is 0.01 m. The initial and boundary conditions are the same as stated in caption of Fig. 4.

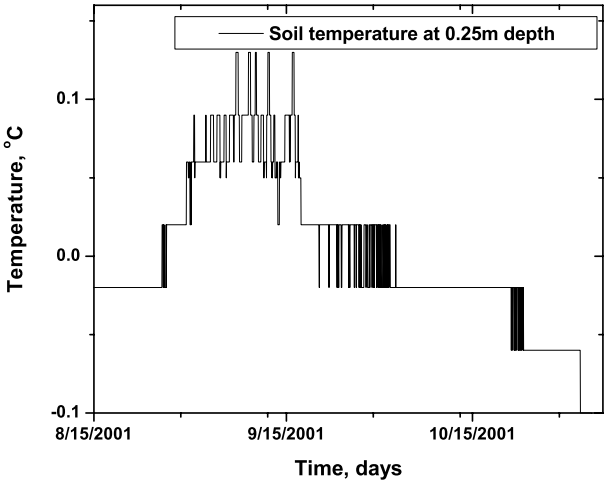

Fig. 7. Temperature dynamics at 0.25 meter depth at Happy Valley site during the summer of 2001 year. The temperature of T_* soil freezing depression can be estimated to be within temperature interval [−0.04°C 0°C].

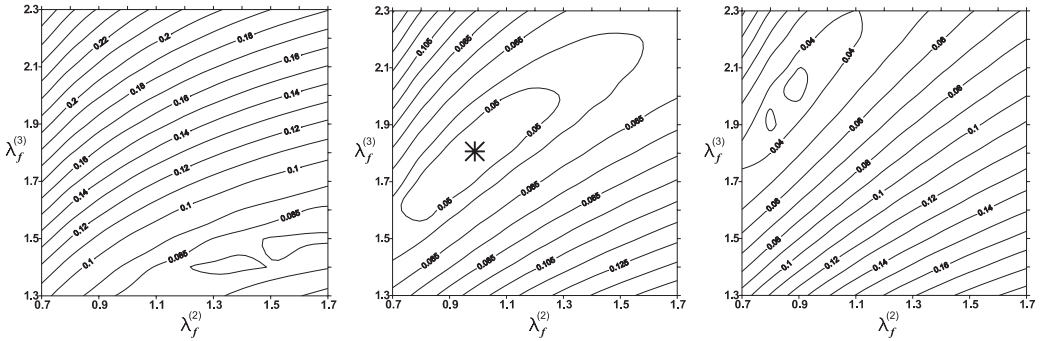

Fig. 8. The isolines of the cost function J on the plane $(\lambda_f^{(2)}, \lambda_f^{(3)})$ for different values of the thermal conductivity $\lambda_f^{(1)}$ keeping constant at each plot. The values of $\lambda_f^{(1)}$ from the left to the right are 0.35, 0.55 are 0.70, respectively. The star in the central plot marks a selected combination of the thermal conductivities.

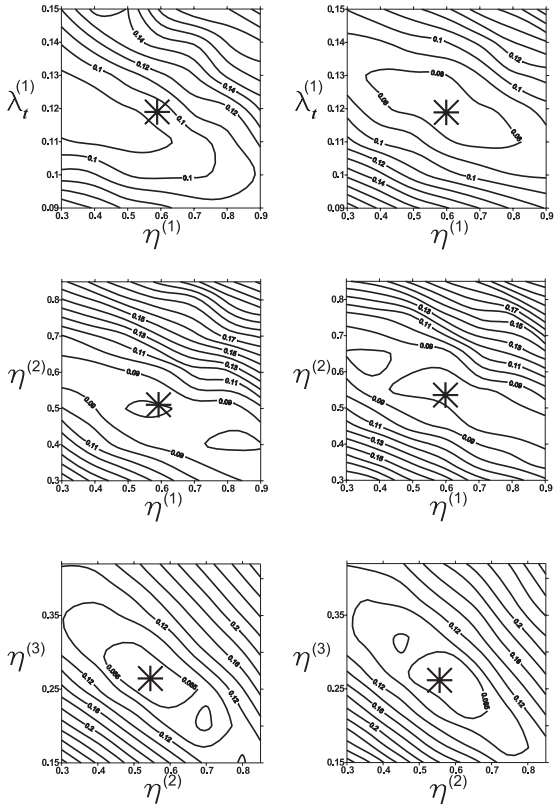

Fig. 9. Selection of the thermal conductivity $\lambda_t^{(1)}$ and the soil porosity $\eta^{(1)}$, $\eta^{(2)}$, $\eta^{(3)}$ by minimizing the cost function associated with the "summer and fall" interval. The left and right column are associated with the first and the second iterations, respectively. The stars mark selected values of parameters after completing the iteration. Note that at the second iteration stars and locations of all minima are coincide.

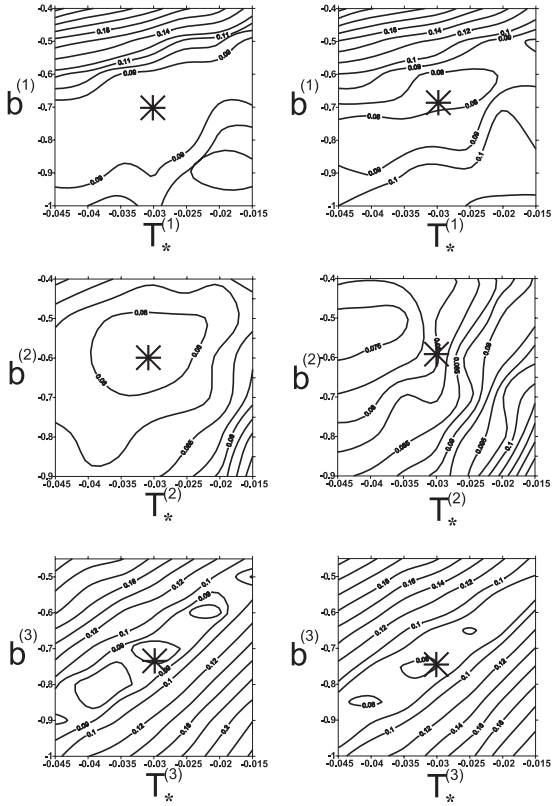

Fig. 10. Selection of the coefficients $\{T_*^{(i)}, b^{(i)}\}_{i=1}^3$ (parameterizing the unfrozen water content) by minimizing the cost function associated with the "fall" interval. The left and right column are associated with the first and the second iterations, respectively. The stars mark selected values of parameters after completing the iteration.

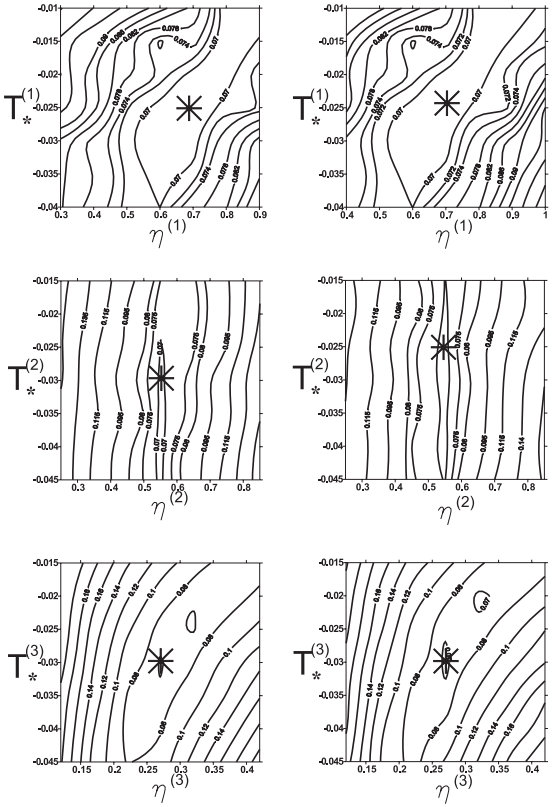

Fig. 11. Selection of the parameters $\{\eta^{(i)}, T_*^{(i)}\}_{i=1}^{3}$ by minimizing the cost function associated with the "extended summer and fall" interval. The left and right column are associated with the first and the second iterations, respectively. The stars mark selected values of parameters after completing the iteration.

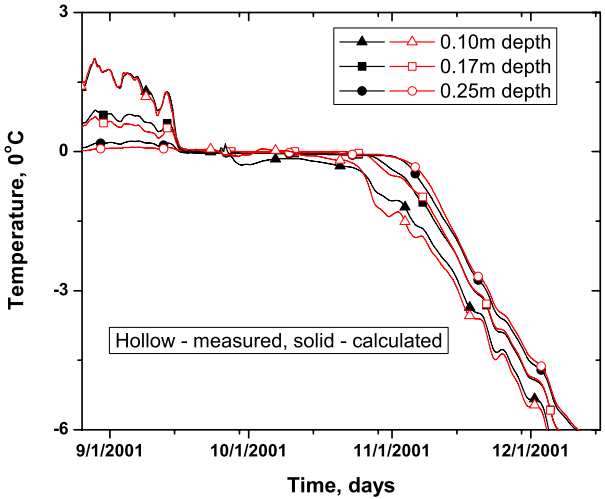

Fig. 12. Measured (hollow) and calculated (solid) temperature at 0.10, 0.17 and 0.25 meter depth. The time interval is associated with the "summer and fall" period.

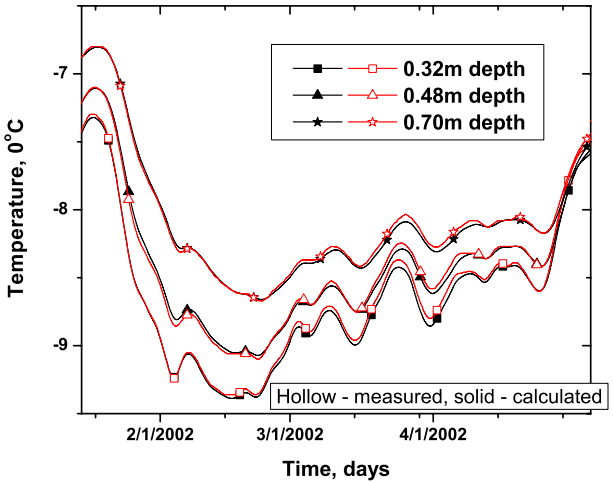

Fig. 13. Measured (hollow) and calculated (solid) temperature at 0.32, 0.48, and 0.70 meter depth. The time interval is associated with the "winter" period.

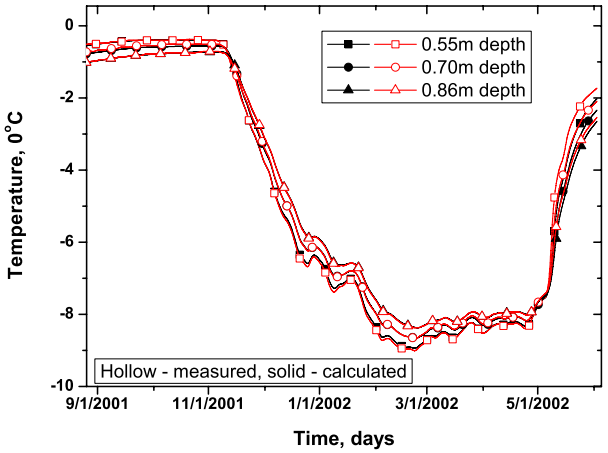

Fig. 14. Measured (hollow) and calculated (solid) temperature at 0.55, 0.70 and 0.86 meter depth during the entire period of measurements used for calibration.

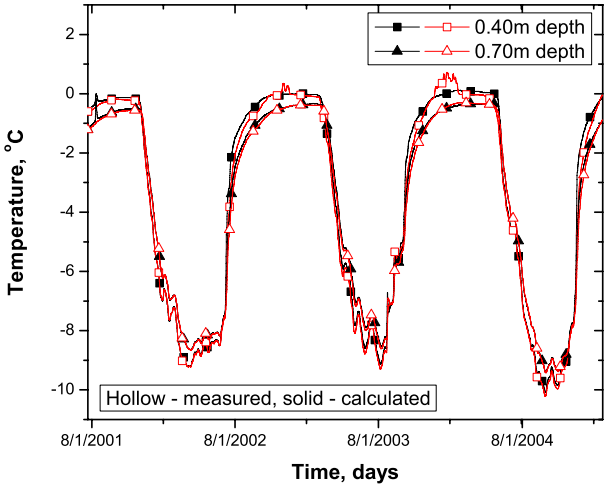

Fig. 15. Measured (hollow) and calculated (solid) temperature at 0.40 and 0.70 meter depth during the entire period of measurements.